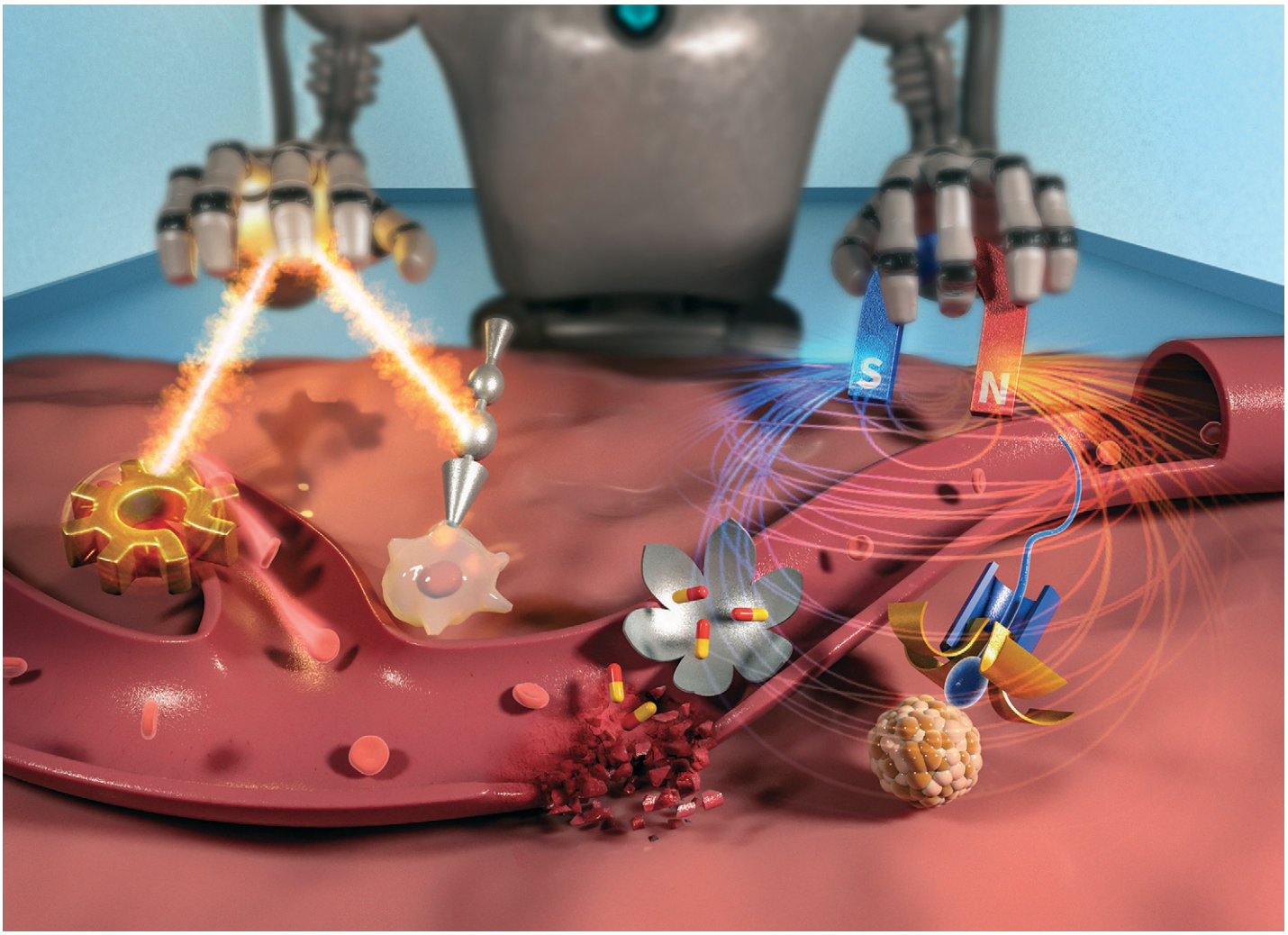

Featuring work from Micro/nano-robotics Research Laboratory of Professor Shuailong Zhang and Professor Huaping Wang, Beijing Institute of Technology, China.

A review on microrobots driven by optical and magnetic fields

Microrobotics technologies have developed rapidly in recent years. This review article comprehensively introduces the working mechanisms, recent progress, and state-of-the-art applications of microrobots driven by optical and magnetic fields.

As featured in:

See Huaping Wang, Shuailong Zhang *et al.*, *Lab Chip*, 2023, **23**, 848.

ROYAL SOCIETY OF CHEMISTRY

rsc.li/loc

Registered charity number: 207890

Lab on a Chip

CRITICAL REVIEW

View Article Online
View Journal | View Issue

Cite this: *Lab Chip*, 2023, **23**, 848

A review on microrobots driven by optical and magnetic fields

Yaozhen Hou,[ab] Huaping Wang, *[abc] Rongxin Fu, [d] Xian Wang,[e] Jiangfan Yu,[fg] Shuailong Zhang, *[abc] Qiang Huang,[abc] Yu Sun[hi] and Toshio Fukuda[b]

Received 24th June 2022,
Accepted 4th November 2022

DOI: 10.1039/d2lc00573e

rsc.li/loc

Due to their small sizes, microrobots are advantageous for accessing hard-to-reach spaces for delivery and measurement. However, their small sizes also bring challenges in on-board powering, thus usually requiring actuation by external energy. Microrobots actuated by external energy have been applied to the fields of physics, biology, medical science, and engineering. Among these actuation sources, light and magnetic fields show advantages in high precision and high biocompatibility. This paper reviews the recent advances in the design, actuation, and applications of microrobots driven by light and magnetic fields. For light-driven microrobots, we summarized the uses of optical tweezers, optoelectronic tweezers, and heat-mediated optical manipulation techniques. For magnetically driven microrobots, we summarized the uses of torque-driven microrobots, force-driven microrobots, and shape-deformable microrobots. Then, we compared the two types of field-driven microrobots and reviewed their advantages and disadvantages. The paper concludes with an outlook for the joint use of optical and magnetic field actuation in microrobots.

Introduction

Microrobotics is an interdisciplinary field that focuses on the design, fabrication and applications of robotic agents with dimensions in the range between 1 μm and 1000 μm.[1–6] Microrobots can be made to do mechanical work and can be classified based on the external fields that drive them, including magnetic,[7–13] electric,[14–17] acoustic,[18–21] and optical

[a] *School of Mechatronical Engineering, Beijing Institute of Technology, Beijing, 100081, China. E-mail: wanghuaping@bit.edu.cn, shuailong.zhang@bit.edu.cn*
[b] *Beijing Advanced Innovation Center for Intelligent Robots and Systems, Beijing Institute of Technology, Beijing, 100081, China*
[c] *Key Laboratory of Biomimetic Robots and Systems (Beijing Institute of Technology), Ministry of Education, Beijing 100081, China*
[d] *School of Medical Technology, Beijing Institute of Technology, Beijing 100081, China*
[e] *Arthur and Sonia Labatt Brain Tumour Research Centre, The Hospital for Sick Children, Toronto, ONT, M5G 1X8, Canada*
[f] *School of Science and Engineering, The Chinese University of Hong Kong, Shenzhen 518172, China*
[g] *Shenzhen Institute of Artificial Intelligence and Robotics for Society (AIRS), Shenzhen 518129, China*
[h] *Department of Mechanical and Industrial Engineering, University of Toronto, Toronto, ON, M5S 3G8, Canada*
[i] *Institute of Biomedical Engineering, University of Toronto, Toronto, ON, M5S 3G9, Canada*

Yaozhen Hou

Yaozhen Hou received the B.S. degree in Mechanical Engineering from Beijing Institute of Technology, Beijing, China, in 2017. He is currently a Ph.D. student at the School of Mechatronical Engineering, Beijing Institute of Technology, Beijing, China. His research interests mainly focus on the fabrication of micro/nano robots and their biomedical applications under magnetic actuation.

Huaping Wang

Huaping Wang received the B.S. degree in Mechatronics and Ph.D. degree in Mechanical Engineering from Beijing Institute of Technology, Beijing, China, in 2010 and 2015, respectively. He was a visiting scholar of Nagoya University, Japan, from 2012 to 2014. He is currently an Associate Professor at Beijing Institute of Technology. His research interests include micromanipulation technologies, micro/nano robotics and microfabrication of biomaterials.

fields.[22–26] Electric field actuation relies on the effective conversion of a system's electric energy into a target's mechanical energy through the interaction of the applied electric field with the target. By controlling the applied electric field, the manipulation force can be effectively exerted on the target to control its movement and position. Acoustic field actuation is another useful method for micromanipulation. The method can be used to control multiple targets simultaneously and accumulate them in desired sites. Acoustic actuation normally requires complex hardware and has limited capability to address targets individually in a crowded environment. Optical field actuation uses optical gradient/pressure forces or other light-induced forces to control the motion of micro-objects. The optical field can be easily modulated to exert manipulation force with high degrees of freedom. Magnetic field actuation relies on the interaction of magnetic-responsive objects with the magnetic field. Magnetic field actuation is highly penetrative and relatively safe to biological samples. Both optical and magnetic fields enable versatile, precise and reliable control of microrobots, which are promising for applications in physics, chemistry, biomedical engineering and other interdisciplinary research. Moreover, the complementarity of optical actuation and magnetic actuation makes their joint use attractive and of great interest to many scientific fields. Therefore, actuation methods and applications of optical and magnetic field-driven microrobots are mainly reviewed in this work.

Optical field-driven microrobots rely on the use of optical micromanipulation technologies, in which optical forces or optically induced forces (dielectrophoretic, thermophoretic, *etc.*) are used to power the microrobots and control their motions. The most widely used optical micromanipulation technology for driving microrobots is optical tweezers (OT),[27–29] which leverage the forces arising from focusing light with strong intensity gradients. OT allow fine and 3D manipulation of the microrobots, but the optical force generated by OT is generally small, in the range of several to several tens of piconewtons (10^{-12} N), which limits the design, fabrication and applications of the microrobots. In addition, it is difficult to perform *in vivo* control and actuation of microrobots using light. Magnetic field-driven microrobots rely on the application of an external magnetic field to impose torque or force on the microrobots, which are made of magnetic-responsive materials and can be made to perform mechanical jobs.[7,8,12,30–32] Due to a wider range of force magnitudes generated by an external magnetic field, magnetic microrobots normally have a wider size range and more flexible physical layouts compared with optical microrobots. To work in a magnetic field, magnetic microrobots must have magnetically responsive materials coated outside or embedded inside the microrobot's mechanical structure. This requirement sets certain limitations on the materials, fabrication and applications of magnetic microrobots. Compared with an optical field, a magnetic field has a better performance to penetrate through the human body, allowing magnetic microrobots to be more easily used for *in vivo* applications such as disease diagnosis and drug delivery.[7,33–36] Magnetic and optical microrobots also share many similarities. For example, both magnetic and optical fields enable long-range, precise, dexterous and robust control of microrobots.[22,23,33,34] In addition, both optical and magnetic microrobots can move in different modes, such as rolling and rotating, to accomplish different tasks in diverse environments.[7,8,22–24,30,31] Some microfabrication techniques, such as photolithography, metallization and two-photon polymerization, can be used to fabricate both optical and magnetic microrobots.[7,12,22–26,30,31,33] These similarities as well as the aforementioned complementarities also promote the joint use of optical and magnetic microrobots for a variety of applications in recent years.

Shuailong Zhang

Shuailong Zhang received the B.S. degree from Beijing Institute of Technology, Beijing, China in 2010, and the Ph.D. degree from University of Strathclyde, Glasgow, United Kingdom, in 2015. He joined the University of Glasgow (UK) and worked as a postdoctoral researcher from 2015 to 2016. In 2017, he moved to Canada and joined the University of Toronto as a postdoctoral fellow. In Aug 2021, he moved to Beijing Institute of Technology and was appointed as a full professor. His current research interests include optoelectronic tweezers, micro/nano robotics, and microfluidic technologies.

Qiang Huang

Qiang Huang received the B.S. and M.S. degrees from the Harbin Institute of Technology, Harbin, China, in 1986 and 1989, respectively, and the Ph.D. degree from Waseda University, Tokyo, Japan, in 1996. In 1996, he joined the Mechanical Engineering Laboratory, Tsukuba, Japan. He was with the University of Tokyo, Tokyo, Japan, from 1999 to 2000. He is currently the Executive Director of the Beijing Advanced Innovation Center for Intelligent Robots and Systems, Beijing Institute of Technology, Beijing, China. His current research interests include bio-robotic systems, human–robot fusion systems, and micro/nano robotics.

This review covers the state of the art of optical and magnetic field-driven microrobots and their related applications, as summarized in Fig. 1. We start by introducing the basic concepts, mechanisms and applications of optical field-driven microrobots, followed by the introduction of the working mechanisms and applications of magnetic field-driven microrobots. Then, we compared and discussed the similarities and differences as well as the pros and cons of the optical and magnetic field-driven microrobots. Finally, we present the recent progress on the joint use of the optical and magnetic field-driven microrobots and discuss the future development of the field.

Recent advances in light-driven and magnetic-driven microrobotics

Optical field-driven microrobot

Light, as an external energy source, is capable of driving the motion of microrobots with the advantages of dynamic programmable, wireless and remote manipulation on demand with high spatial and temporal resolution. Light-driven microrobots can be sub-classified into three categories based on their operating principles. The first category, known as optical field-driven microrobots, relies on the use of optical micromanipulation technologies that can control and modulate an optical field or other physical fields to impose actuation force on microrobots.[22–26] The second category, known as opto-soft microrobots, relies on the interaction between light and artificial muscle made of photosensitive, mechanically responsive soft materials such as liquid crystal polymers (LCPs).[37–42] The third category, opto-chemical microrobots, relies on photochemical reactions to generate propulsion forces, thus converting chemical energy into mechanical movement.[43,44] Opto-soft microrobots and opto-chemical microrobots have been comprehensively overviewed in previous review articles[41–44] and we will mainly introduce the optical field-driven microrobots in this work.

Microrobots driven by optical tweezers. OT are a revolutionary micromanipulation technology invented by Arthur Ashkin in 1980s, which brought him one half of the Nobel Prize in Physics in 2018. OT has continuously evolved and helped revolutionize scientific research by providing non-contact, non-invasive and precise manipulation of micro-/nano-sized objects. To date, OT has been used in many fields of natural science, ranging from cell/virus manipulation,[45–47] characterization of biomolecules and biosystems,[48,49] micro-/nano-assembly,[50,51] to trapping and cooling atoms.[52,53] In recent years, several groups have

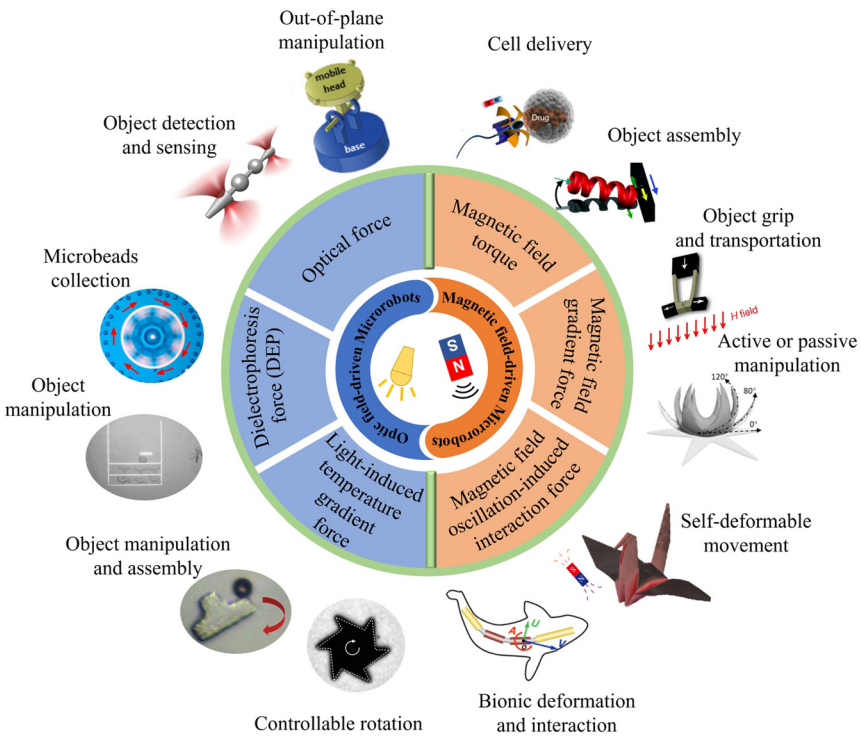

Fig. 1 Schematic illustration of optical and magnetic field-driven microrobots and their related applications. Reproduced with permission from ref. 68. Copyright 2017, John Wiley & Sons, Inc. Reproduced with permission from ref. 73. Copyright 2014, Springer Nature Limited. Reproduced with permission from ref. 83. Copyright 2021, Springer Nature Limited. Reproduced with permission from ref. 84. Copyright 2017, John Wiley & Sons, Inc. Reproduced with permission from ref. 96. Copyright 2019, John Wiley & Sons, Inc. Reproduced with permission from ref. 100. Copyright 2015, Springer Nature Limited. Reproduced with permission from ref. 107 Copyright 2020, American Association for the Advancement of Science. Reproduced with permission from ref. 112. Copyright 2018, American Chemical Society. Reproduced with permission from ref. 119. Copyright 2014, Royal Society of Chemistry. Reproduced with permission from ref. 137. Copyright 2014, John Wiley & Sons, Inc. reproduced with permission from ref. 138. Copyright 2021, Nature Publishing Group. Reproduced with permission from ref. 150. Copyright 2016, John Wiley & Sons, Inc.

started to investigate the use of OT to control micromechanical structures for different applications, leading to the invention and fast development of optical microrobots. OT relies on the transfer of momentum from a photon to a particle when laser light interacts with the object, which can be trapped near the beam focus due to the intensity gradient force. In addition, optical radiation pressure force, resulting from the absorption and scattering of light by the object, also plays an important role. By carefully balancing the optical gradient force and optical radiation pressure force in OT, the position of the sample can be controlled in three-dimensional space,[54] as shown in Fig. 2(a). Light also carries angular momentum. For example, in a circularly polarized optical field, the electric field vector is rotating in a plane perpendicular to the moving direction of the wave. If the object can change the polarization state of the light (from circularly polarized to linearly polarized),[55] a torque will be exerted on the object and make it spin due to the conservation of momentum. The hardware of the OT system normally consists of a laser source, an optical microscope and lenses that can collimate the laser beam.

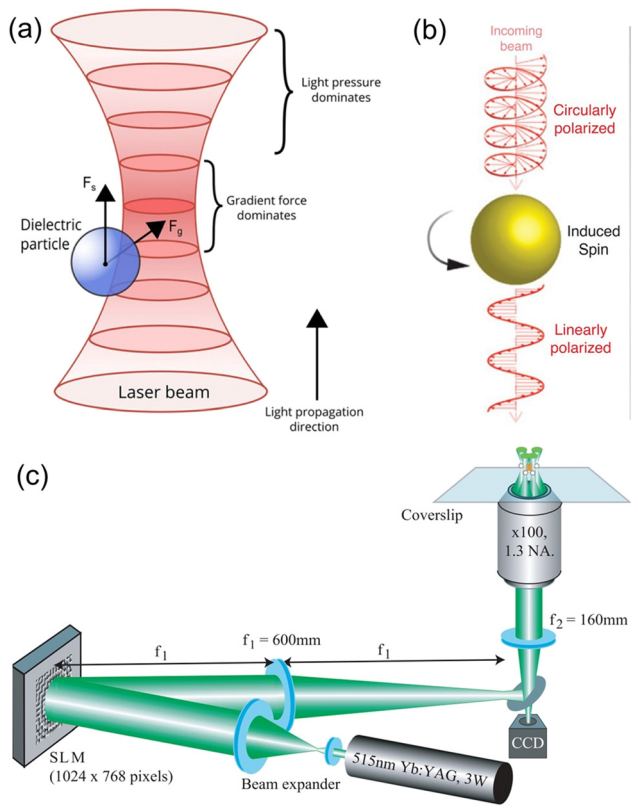

Fig. 2 Working mechanisms of OT. (a) Schematics illustrating the working mechanisms of OT, in which a dielectric particle experiences optical gradient force and optical radiation pressure force (reproduced with permission from ref. 54. Copyright 2015, John Wiley & Sons, Inc.). (b) Transfer of optical angular momentum to an object, leading it to spin (reproduced with permission from ref. 55. Copyright 2018, Wiley-VCH GmbH). (c) Schematic experimental setup for holographic OT, which can trap multiple targets simultaneously (reproduced with permission from ref. 56. Copyright 2006, Optica Publishing Group).

The laser is normally linearly polarized but can be converted into a circularly polarized state carrying angular momentum using a quarter-wave plate. For the manipulation of microrobots, holographic OT that can generate multiple Gaussian light beams are widely used,[56,57] as shown in Fig. 2(c). Holographic OT allow the control and manipulation of multiple microrobots simultaneously and enables the stable control of microrobots by providing a holding force at multiple points.

Presented in Fig. 3 are examples of OT-actuated microrobots with different designs, mechanical structures and functions. These microrobots have small feature sizes (a few microns to a few tens of microns) and were mostly fabricated using microfabrication techniques such as electron-beam lithography, wet or dry etching, and two-photon photo-polymerization (2PP). Shown in Fig. 3(a) is a schematic of an OT-actuated birefringent microrobot.[58] Its detailed mechanical structure is illustrated in Fig. 3(b), which resembles a microgear but consists of nano-sized trenches in the middle. On applying a circularly polarized light beam, the microrobot is capable of rotating at a controllable rate by functioning as a half-wave retardation plate to harvest angular momentum from the light beam. Similar results were reported for other birefringent micromotors, as shown in Fig. 3(c) and (d). By placing the spinning micromotor close to the growth cone of the nerve fiber, the localized microfluidic flow generated by the spinning micromotor can exert fluidic shear force on the nerve fiber and influence its growth direction.[59] By changing the rotation direction and position of the spinning micromotor, the direction of nerve fiber growth can be precisely manipulated and guided. Microfluidic flow generated by light-driven micromotors was also used to disrupt and break apart aggregates of microparticles and cells, as shown in Fig. 3(e). In this work, spinning micromotors consisting of living cells are used to generate a localized microfluidic flow to break apart SiO_2 particle aggregates and blood clots.[60] Transmission of torque at the nanoscale is made possible by a light-driven disc-like colloidal assembly, as shown in Fig. 3(f) and (g). Twenty-seven microparticles in optical traps are translated on a circular path to form a rotating boundary, which can transmit torque to additional microparticles in the middle.[61] It is found that the transmission behaviour is predominantly governed by the rotation rate of the boundary and the density of the confined system. It is worth mentioning that there are many examples of spinning microrobots actuated by OT, which were used to generate micro-vortex and exert hydrodynamic forces to manipulate or influence surrounding objects.[62–65] To enhance the conversion efficiency of optical energy to rotational movement, microrobots with beam-shaping structures that can reroute the input light beam and efficiently harvest the optical momentum were also designed, fabricated and demonstrated for various studies.[66,67] The use of OT-actuated rotatable microrobots to induce hydrodynamic forces for indirect optical manipulation is an interesting topic that has attracted much research interest in recent years. This approach expands the capabilities of OT technology for the manipulation of fragile

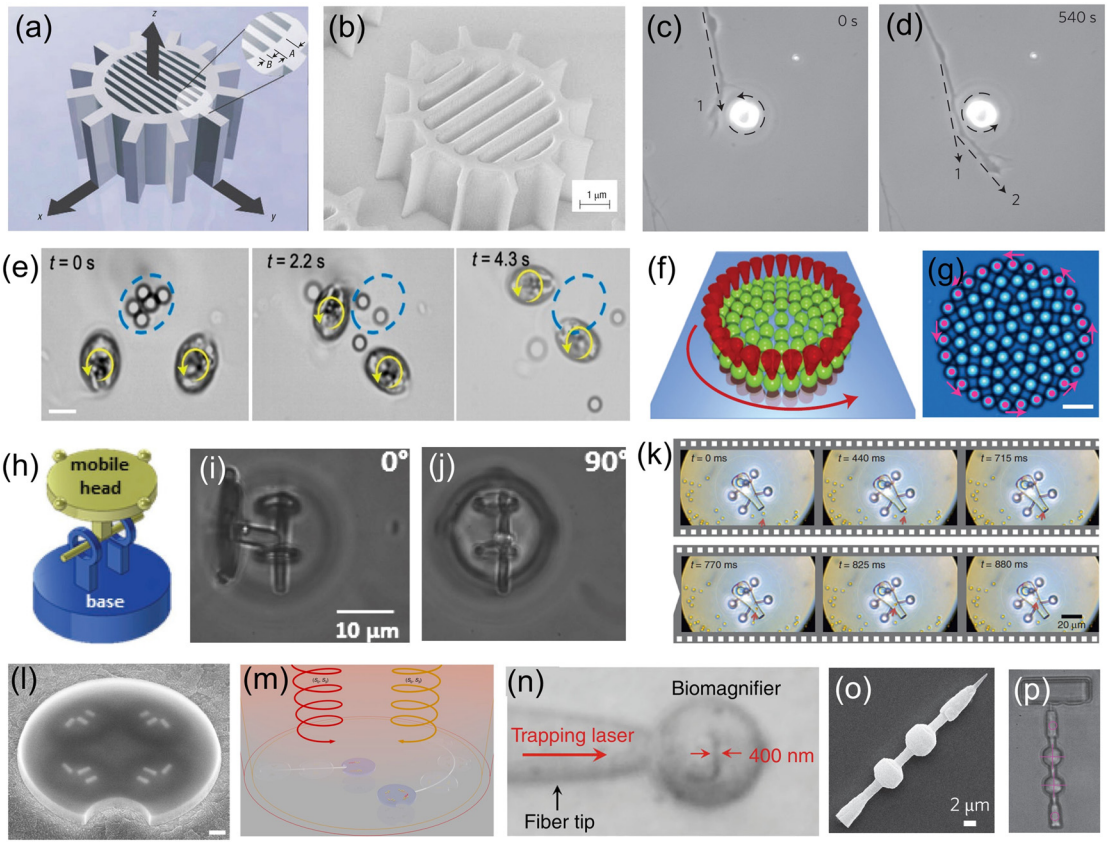

Fig. 3 OT-actuated microrobots. (a) Schematic model of birefringent microrobot. (b) Scanning electron microscopy (SEM) image of the fabricated birefringent microrobot (reproduced with permission from ref. 58. Copyright 2005, Nature Publishing Group). (c) and (d) Time-lapse images showing the use of a birefringent rotating micromotor to control the direction of growth of nerve fibers (dashed arrow) (reproduced with permission from ref. 59. Copyright 2012, Nature Publishing Group). (e) Time-lapse images showing the use of two rotating cell-based micromotors to break apart SiO_2 particle aggregate (reproduced with permission from ref. 60. Copyright 2020, American Chemical Society). (f) and (g) Schematic and microscope image of the nano-clutch. Red cones represent optical traps translating 27 microparticles on a circular path (counter-clockwise rotation) (reproduced with permission from ref. 61. Copyright 2016, Nature Publishing Group). (h) Schematic of an articulated microrobot. (i) and (j) Out-of-plane rotation of the mobile head of the articulated microrobot with respect to various angles (reproduced with permission from ref. 68. Copyright 2016, Wiley-VCH GmbH). (k) Time-lapse images showing the process of loading cargo into the microrobot (reproduced with permission from ref. 70. Copyright 2016, Nature Publishing Group). (l) SEM image of a microdrone with four nanomotors. (m) Schematic of using light beams with different wavelengths and polarization states to drive the microdrones (reproduced with permission from ref. 71. Copyright 2022, Nature Publishing Group). (n) Microscope image showing the light-actuated bio-magnifier that can image a nanopatterned letter (reproduced with permission from ref. 72. Copyright 2019, Nature Publishing Group). (o) SEM image of a surface scanning probe and (p) optical image of the probe as it scans the surface of a sample (reproduced with permission from ref. 73. Copyright 2014, Nature Publishing Group).

and light-sensitive biological samples that are difficult to manipulate by OT directly.[62]

OT can also be used to drive microrobots in 3D to perform out-of-plane movements. As shown in Fig. 3(h), an articulated microrobot is fabricated using the 2PP technique, which consists of a fixed base and a mobile head.[68] OT allows robust and out-of-plane control of the robot's mobile head with respect to various angles, as shown in Fig. 3(i) and (j). Similar results were also demonstrated for a screw-wrench structure.[69] Another application of OT-actuated microrobots is cargo transport and delivery.[70] Fig. 3(k) demonstrates a microrobot equipped with a syringe function. This microrobot has a hollow body with four spheroidal handles, which were fabricated using the 2PP technique. The body of the microrobot has two openings; one serves as the spout where cargo can be loaded and ejected, and the other one is located on top of the microrobot, allowing for the generation of photothermally induced convection currents within the body of the microrobot. This OT-actuated microrobot is capable of loading, transporting and unloading cargo such as dielectric microbeads. For this microrobot, laser beams were used to provide actuation force and to generate photothermally induced convection currents for unloading cargo. More recently, light-driven microdrones were also developed, which can be maneuvered in two dimensions in all three independent degrees of freedom using two laser beams with different wavelengths and circular polarization states.[71] Fig. 3(l) shows the SEM image of the microdrone, which consists of individually addressable chiral plasmonic nano-antennas acting as nanomotors. These nanomotors can resonantly scatter the driving light into well-defined directions and produce optical recoil forces to drive the

microdrone, as shown in Fig. 3(m). Therefore, the microdrones can be maneuvered by adjusting the optical power for each nanomotor, and this actuation concept resembles that of macroscopic multirotor drones. Fig. 3(n) shows an OT-actuated cell-based microrobot, which was trapped on a fiber tip.[72] Due to the spherical structure, the cell can act as a bio-magnifier to overcome the optical diffraction limit and probe nanostructures with a resolution of 100 nm. In addition, the focus of the bio-magnifier forms a nano-optical trap that allows precise manipulation of individual nanoparticles with a radius of 50 nm. Therefore, this cell-based OT-actuated bio-magnifier is a useful tool for both optical imaging and assembly of nanomaterials. Shown in Fig. 3(o) is an OT-actuated surface scanning probe.[73] By using two laser beams to control and manipulate the probe [Fig. 3(p)], it can be applied for surface topography reconstruction with sub-micron resolution. Another surface scanning probe capable of manipulating a light field was also developed.[74] Different tip structures of the probe can be fabricated to modulate the light field and generate light beams with different profiles, helping to break through the optical diffraction limit for ultra-sensitive optical detection and sensing applications. The fast development of OT and the microfabrication technologies provide a solid technical foundation for these optical microrobots, allowing fabrication of microrobots with different designs and functions for many useful applications.

Microrobots driven by optoelectronic tweezers. Microrobots actuated by OT have been demonstrated for many impressive applications as introduced above, but there still exist some limitations for this type of system. First, OT are capable of actuating only small objects as the optical force is typically on the order of piconewtons (10^{-12} N). This restricts the design, structure, materials and tools used to fabricate the microrobots and sets limits on their applications. Second, while it is possible to manipulate multiple microrobots in parallel with OT, this functionality requires dramatic increases in complexity, as it necessitates specialized and expensive beam-modulation hardware and control software. To overcome these limitations, substantial efforts have been devoted to the development of other optical micromanipulation technologies, such as optoelectronic tweezers (OET).

OET is a powerful optical micromanipulation technology invented by Ming C. Wu and co-workers in 2005.[75] Based on light-induced dielectrophoresis (DEP) force, OET combines the merits of optics and electronics and offers a user-friendly approach that enables programmable, touch-free and reliable manipulation of micro-/nano-sized objects.[76] Different from OT which require a coherent laser light source with high optical intensities, the optical source in an OET system can be a digital micromirror device (DMD) with a LED,[77,78] which is used to project animated light patterns onto a photoconductive substrate [in most cases, hydrogenated amorphous silicon (a-Si:H)]. OET relies on the unique features of the photoconductive substrate: in the dark, the impedance of the photoconductive substrate is high and it behaves like a resistor; when the photoconductive substrate is illuminated with light, its impedance is reduced significantly and the photoconductive substrate behaves like a conductor. Therefore, by creating bright and dark regions on the photoconductive substrate, "virtual electrodes" are formed, which can induce a non-uniform electric field in the liquid medium above the photoconductive substrate, as shown in Fig. 4(a). This non-uniform electric field interacts with the samples in the liquid medium, producing a DEP force that can control their positions.[79] Compared with OT, OET is capable of exerting a stronger manipulation force (nanonewtons, 10^{-9} N) to actuate larger objects (sizes over 100 microns) and, in addition, well suited for parallel manipulation (*e.g.* creating 10 000 traps at the same time). These features make OET an ideal optical tool to control multiple microrobots in parallel and also microrobots with large feature sizes. Presented in Fig. 4(b) is an example of an OET-actuated "cogwheel"-shaped microrobot.[82] The microrobot is more than 200 μm and can be massively fabricated using UV-curable polymer materials and standard photolithography technique. By using a light pattern that forms a negative relief of the perimeter of the microrobot, negative DEP force is produced, causing the microrobot to be trapped in the "dark" central region of the projected light pattern. By moving the light pattern, the "cogwheel"-shaped microrobot can be programmed to move, rotate and carry out sophisticated, multi-axis operations. One particularly useful program demonstrated here [Fig. 4(c) and (d)] is a serial combination of "load", "transport," and "deliver," which can be applied to manipulate micron-dimension payloads such as mammalian cells. It has been demonstrated that the microrobot programmed in this manner can cause less stress on fragile biological samples than directly using the OET technique. Besides, a key feature of this OET-actuated microrobotic system is the capability to manipulate multiple microrobots simultaneously, allowing for independent and parallel control. This OET-actuated microrobot is also multi-functional, with applications demonstrated for single-cell isolation, clonal expansion, RNA sequencing, cell–cell fusion, and isolating precious microtissues from heterogeneous mixtures. Presented in Fig. 4(e) is a schematic of a "cogwheel"-shaped micromotor relying on OET.[83] This micromotor can be precisely rotated to generate localized hydrodynamic forces to control the motion of micro-objects in their vicinity, as shown in Fig. 4(f). In an advance relative to the state of the art, multiple micromotors can be made to work together as micromachines. For example, two rotating micromotors can be used as a touchless microfeed roller to control microparticle movement in 3D. In addition, the motions of multiple micromotors can be effectively coupled together to form a variety of micromechanical systems. Fig. 4(g) shows a micro-gear train consisting of an active micromotor and a passive micromotor. This micro-gear train works by driving the rotation of one micromotor with OET and then using the torque generated by this active process to

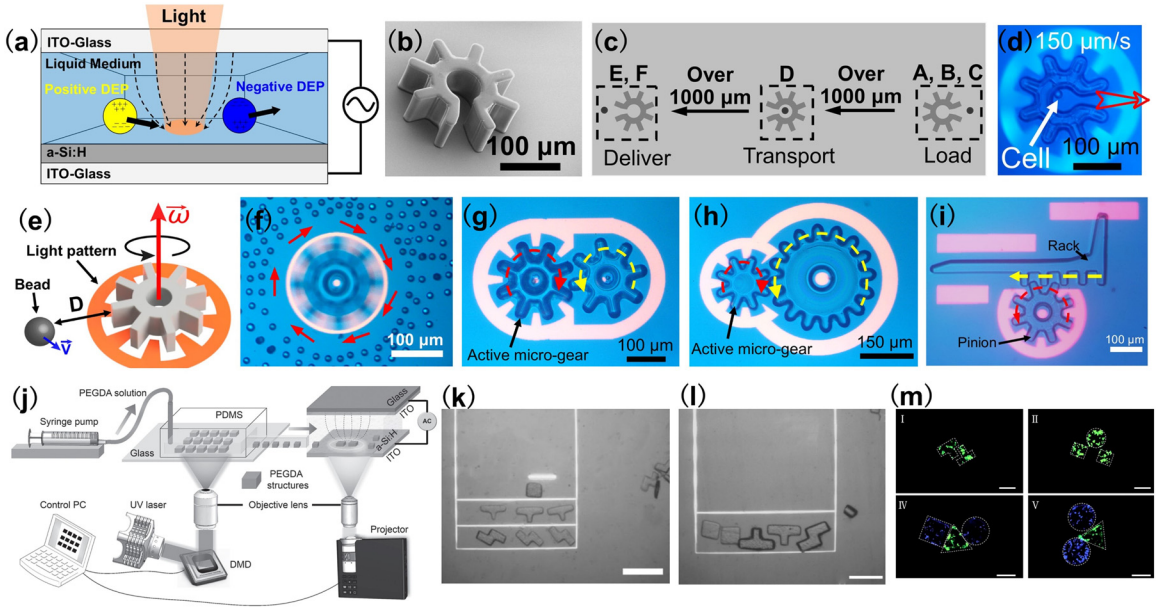

Fig. 4 OET-actuated microrobots. (a) Schematic of OET. (b) SEM image of a "cogwheel"-shaped microrobot. (c) Schematic process of loading, transporting, and delivery of payloads using OET-actuated microrobots. (d) Microscope image showing the use of light pattern to move a "cogwheel"-shaped microrobot at 150 μm s^{-1}, which carries a cell (reproduced with permission from ref. 82. Copyright 2019, Nature Publishing Group). (e) Schematic of a rotating micro-gear and its influence on a nearby particle. (f) Microscope image of a rotating micromotor on nearby 15 μm-diameter polystyrene microbeads. (g) Microscope image of a micro-gear-train driven by one active micro-gear comprising two micro-gears. (h) The micro-gear train formed from small (150 μm diameter) and large micro-gears (300 μm diameter). The small micro-gear drives the system. (i) A micro-rack-and-pinion system in operation, in which rotating the pinion counterclockwise can make the rack translate to the left (reproduced with permission from ref. 83. Copyright 2021, Nature Publishing Group). (j) Schematic illustration of the hydrogel fabrication and OET manipulation system. The system consists of two major components: a DMD-based hydrogel fabrication system and an OET-based manipulation and assembly system. (k) and (l) Assembly of Tetris hydrogel microrobots with OET. Scale bar: 50 μm. (m) Fluorescence microscope image showing the assembly of cell-encapsulating Tetris hydrogel microrobots. L929 fibroblast cells were stained green and HEK-293 cells were stained blue. Scale bar: 100 μm (reproduced with permission from ref. 84. Copyright 2017, John Wiley & Sons, Inc.).

drive the rotation of another passive micromotor. Therefore, mechanical momentum can be transferred from one micromotor to another. To test the capacity to form torque multipliers with mechanical advantage (MA) >1, micromotors with varying sizes were formed and assembled into a micro-gear train, as shown in Fig. 4(h). In this case, MA = 2 and the micro-gear train amplifies the input torque twofold. OET-driven micro-gear train system is also reconfigurable, allowing users to adjust the number of active and passive micromotors in the system and the layouts as well as the MA of the system. In addition to micro-gear train that can convert rotation to rotation, micro-rack-and-pinion that can convert rotation to linear movement was also developed, as shown in Fig. 4(i). In combination with microfluidic structures, the micro-rack-and-pinion can be used as a valve to control the flow within microfluidic channels. These sophisticated micromechanical systems are unique to what have been reported previously and suggest great potential for building complex microrobotic systems in the future for applications in micromanipulation, microfluidics, and beyond.

In addition to polymer-based microrobots, shown in Fig. 4(j)–(m) are examples of hydrogel microrobots with Tetris structures, which were manipulated and assembled by OET.[84] Using a DMD-based UV curable system [Fig. 4(j)],[84,85] microrobots made of UV-curable hydrogel can be fabricated into different Tetris structures by projecting UV light patterns to the hydrogel. After the fabrication, the hydrogel microrobots can be assembled to form desired combinations using OET, as shown in Fig. 4(k) and (l). The hydrogel microrobots have high biocompatibility and can encapsulate cells with different species. Therefore, hydrogel microrobots containing different cells can be assembled to form the desired geometry with a specific shape and size, as shown by the fluorescence microscope images in Fig. 4(h). These hydrogel microrobots are useful for a variety of applications such as microscale tissue engineering, drug screening and studying cell–cell interactions.

The commercialization of OET technology started in 2011.[86] Ming Wu, the inventor of OET, founded Berkeley Lights Inc. together with Igor Khandros and William Davidow.[76] This California-based company has successfully commercialized fully automated OET instruments to enable the functional screening and selection of individual cells for antibody discovery,[87,88] cell line development,[89,90] cell therapy development[91] and synthetic biology.[92]

Microrobots driven by heat-mediated optical manipulation techniques. Apart from OT and OET, optical micromanipulation techniques based on an optically induced temperature gradient can also be used to control and

manipulate microrobots. Through rational design of the light-generated temperature gradient and exploring the mechanical response of microrobots to the temperature gradient, a variety of microrobots were developed and used for micromanipulation and micro-assembly applications.[93,94] Shown in Fig. 5(a) is a microrobot with a rocket-like triple-tube structure. When near-infrared (NIR) laser excites the microrobot, its tail's temperature is significantly higher than that of the head, resulting in an asymmetric temperature gradient and the thermophoretic force that pushes the microrobot forward.[95] Owing to the increasing quantity of the propulsion channel and the light-excitation interfacial area, the rocket-like microrobot can reach a moving speed of 2.8 mm s^{-1} under NIR actuation in a blood-mimicking viscous glycerol solution. This microrobot could also be applied *in vivo*, such as the ear of a mouse, where it could be tracked *via* photoacoustic imaging. Other microrobot examples based on an optothermal actuation mechanism are shown in Fig. 5(b)–(f). In this work,[96,97] a laser focus on a photothermal substrate creates a surface bubble, which can be used as a microrobot to translate, rotate, lift, and drop micro-parts and assemble them into an interconnected entity. By controlling the power and the position of the laser beam, the generation, growth rate and motion of the bubble microrobot can be well controlled. In addition, the bubble microrobot can be used to move and assemble microgel blocks consisting of living cells, with applications demonstrated for microtissue fabrication and studying cancer metastasis.[98,99] Fig. 5(g) shows an asymmetric microrobot structure, which was coated with a layer of light-absorbing material and sitting on a liquid–air interface.[100] By illuminating the microrobot with incoherent light, it can efficiently convert absorbed light into rotational motion through thermocapillary convection (also known as Marangoni convection), as shown in Fig. 5(h). It is worth mentioning that there are many other reports of using heat-medicated optical micromanipulation techniques to drive microrobots in fluidic environments.[93] We believe that with the development and further improvement of different optical micromanipulation technologies, more types of microrobots will be invented and various applications will be explored. It is expected that field-driven microrobots based on optical micromanipulation technologies and tailored physical fields will continue to thrive and play important roles in a wide range of applications in physics, engineering, biomedical science and beyond.

Magnetic field-driven microrobots

Microrobots driven by a rotating magnetic field. Magnetic actuation relies on the use of magnetic force and torque to manipulate magnetized micro-object.[101] A magnetized object in a rotating magnetic field experiences a torque T_m [N m] that is determined by the cross product of magnetization M [A m^1] and the external field B [T], which can be expressed as

$$T_m = VMB \quad (1)$$

in which V [m^3] represents the volume of the magnetic object. When a microrobot is placed in a rotating magnetic field, it can rotate in response to the magnetic torque induced by the rotating magnetic field and generate propulsion force in due course. Compared with microrobots actuated by magnetic field gradients and oscillating magnetic fields, the microrobots driven by rotating magnetic fields show superior performance in maneuverability and precise locomotion and can work with

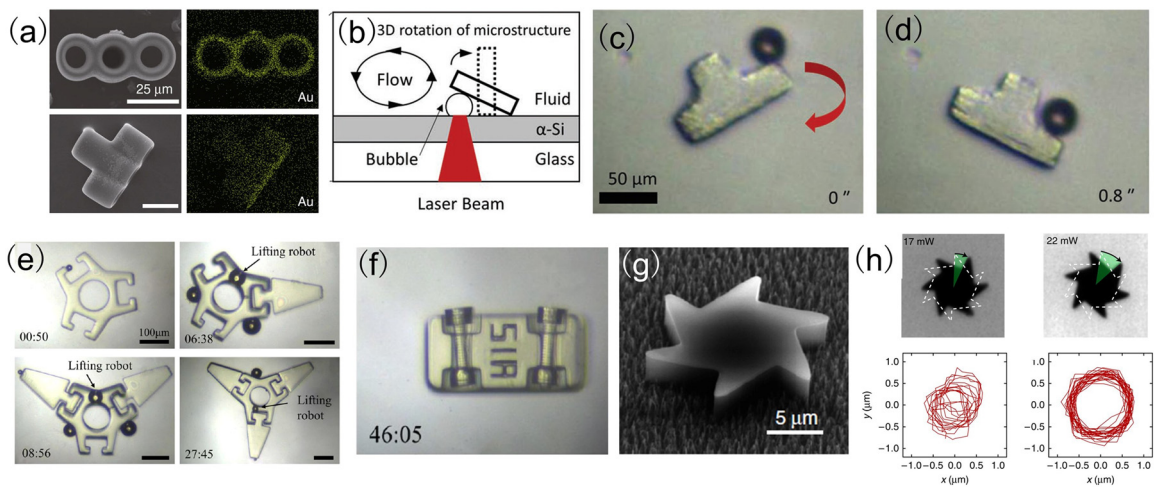

Fig. 5 Microrobots actuated by heat-mediated optical micromanipulation techniques. (a) The top view and side view of the energy-dispersive X-ray spectrum (EDS) mapping of a micro-rocket (reproduced with permission from ref. 95. Copyright 2020, Nature Publishing Group). (b) Schematic setup to generate a bubble microrobot using a laser beam. (c) and (d) The rotation of a convex structure using a bubble microrobot (reproduced with permission from ref. 96. Copyright 2019, John Wiley & Sons, Inc.). (e) Assembly of micromechanical parts using bubble microrobots. (f) Assembly of the vehicle structure using bubble microrobots (reproduced with permission from ref. 97. Copyright 2020, American Chemical Society). (g) SEM image of a micromotor with an asymmetric shape. (h) Rotational and translational trajectories of the micromotor for a total time interval of 5 seconds (reproduced with permission from ref. 100. Copyright 2015, American Chemical Society).

magnetic fields with limited field strength. For a rotating magnetic field, it can be characterized by a field vector rotating continuously around an axis,[102] as shown in Fig. 6(a).

For microrobots actuated by a rotating magnetic field, their design and fabrication process are important for their moving performance and practical applications. Helical-structured microrobots are the most widely used ones to work with rotating magnetic fields. For such microrobots, they rotate around the helical axis and move forward in the direction perpendicular to the rotation plane of the microrobot. Similar to helical microrobots, magnetized spherical microrobots can also be easily actuated by rotating magnetic fields,[103] as shown in Fig. 6(b). To fabricate the microrobots driven by rotating magnetic fields, microfabrication methods such as self-scrolling, direct laser writing (DLW) and bio-templating synthesis[103–105] are widely used to endow the microrobots with good biocompatibility and suitability for locomotion and carrying payloads.

Shown in Fig. 7(a)–(e) are examples of microrobots with different designs and functions actuated by rotating magnetic fields. The prototype of the magnetic helical microrobot was first proposed by Honda *et al.* in 1996,[106] which is made of a cubic magnet attached to a spiral copper wire. The helical microrobot is an ideal model to investigate the swimming behaviors of microrobots in a liquid environment with low Reynolds numbers. Since then, many useful applications have been developed based on helical microrobots, such as drug delivery,[107–109] cargo transportation,[110–112] cell co-culture,[113,114] and micro-object assembly.[115–117] Fig. 7(a) shows an artificial sperm-hybrid microrobot[112] consisting of a motile sperm cell and a 3D-printed magnetic "tetrapod". The sperm cell provides the propulsion source and serves as a drug carrier, while the 3D-printed "tetrapod" can experience magnetic force and guide the movement of the hybrid microrobot. In an *in vitro* experiment, the sperm-hybrid microrobot was guided to move toward HeLa cells using a rotating magnetic field. When the microrobot physically touches the HeLa cell surface, it experiences a shape change and the sperm cell carrying the drug is separated from the "tetrapod" head and released into the surrounding environment. Then, the swimming sperm cell can physically interact with the HeLa cells and deliver the drug precisely. Compared to conventional drug delivery methods, this new method based on sperm-hybrid microrobots exhibits superior performance in drug delivery and killing targeted cancer cells. Although this drug delivery method based on sperm-hybrid microrobots is challenging to apply for *in vivo* environments, it is expected that this method would be of great use for many *in vitro* biomedical applications such as disease diagnosis and biochemical analysis.

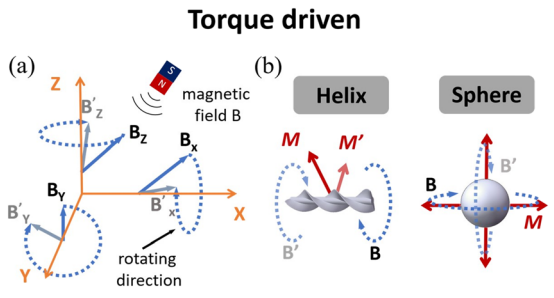

Fig. 6 (a) Schematic of rotating magnetic field actuation. The magnetic fields can rotate around three axes of the coordinate to achieve 3D actuation. (b) There are two typical models, helix and sphere, which show different motion modes under the rotating magnetic fields.

Rotating magnetic field-driven microrobots can also be used to do different mechanical jobs, such as gathering, releasing, detecting and assembling.[118–121] Fig. 7(b) shows a helical microswimmer with a half-cylindrical head and a helical tail.[118] The microrobot was fabricated by two-photon photolithography (TPP) and coated with thin layers of nickel (Ni) and germanium (Ge) by electron beam evaporation. After the deposition of the Ni layer, the microrobot becomes magnetically responsive and can be effectively manipulated by a magnetic field. The flat surface of the microswimmer's head has nanostructures. When integrated with a thin layer of Ge, the flat surface can express strong light reflection with different colours for easy observation. The periodic arrangement of the nanostructures plays an important role in the colour expression of the reflected light. This approach increases the visibility of the microrobots, providing a useful solution for real-time tracking of the microrobot with potential applications for biolabeling, biosensing and medical therapy. Another type of helical microrobot is shown in Fig. 7(c). These microrobots were fabricated using 3D direct laser writing (DLW) and deposited with a thin layer of Ni and Ti *via* electron beam evaporation.[119] The helical microcarrier has ring-shaped microstructures, which increases the contact area between the microrobot and the surface, allowing it to move smoothly without wobbling. For cargo transportation and object assembly, multiple microrobots can work together to reliably load and unload target objects through generating pushing forces or rotation-induced frictional forces. This work provides an insightful solution for parallel control of multiple microrobots to achieve multi-DOF manipulation of arbitrarily shaped micro-objects in 3D, which are useful for micro-assembly and target delivery tasks. Fig. 7(d) shows a piston-like microrobot with a shaft that can actively rotate to generate a fluidic vortex and load particles into the cylinder cavity *via* hydrodynamic force.[120] The whole body of the microrobot was fabricated using 3D laser writing and the shaft was coated with an additional layer of Ni/Ti. This piston-like microrobot can load and release a lot of micro-objects into the cylinder cavity simultaneously and was demonstrated to be useful for transporting micro-particles, cells and microtissues. By optimizing mechanical structures, functionalizing the surface and using soft bio-compatible materials, it is expected that this microrobot can be further improved for *in vivo* targeted drug delivery or performing complex tasks in the microscopic world such as mechanical removal of occlusions, collection of biological samples and generation of a localized fluidic

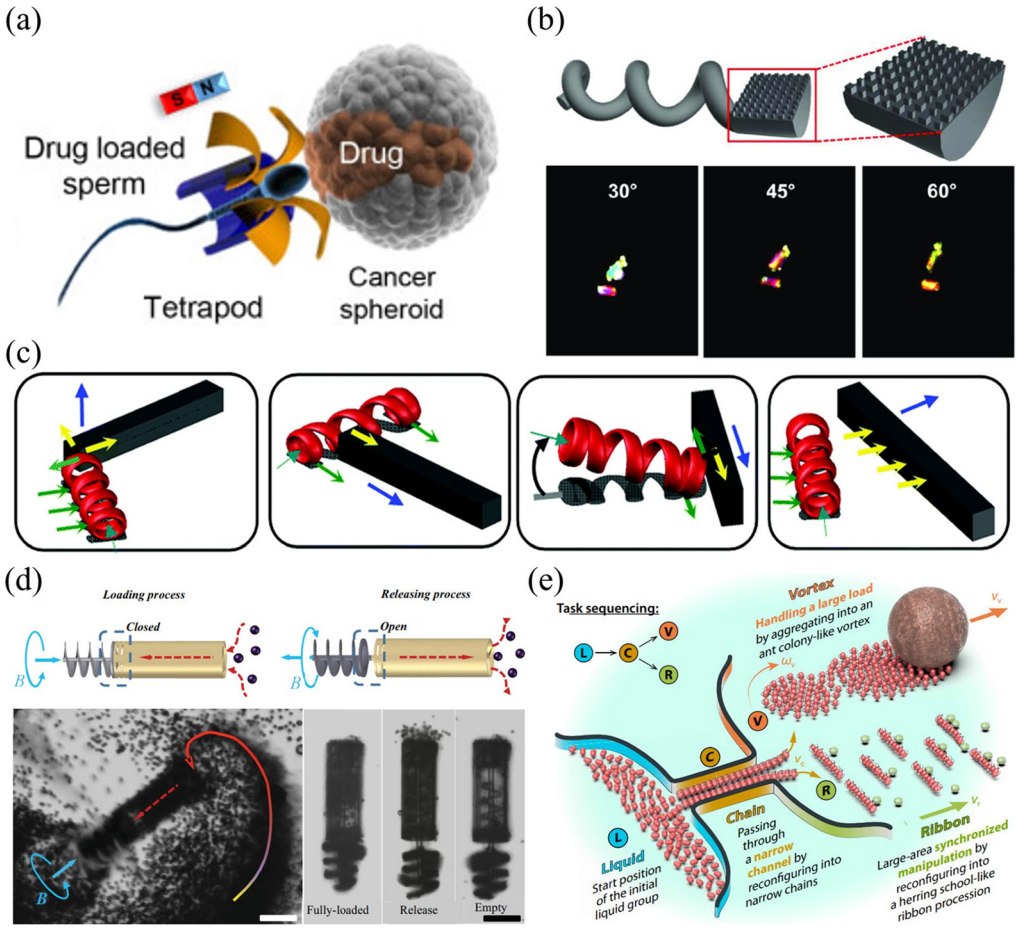

Fig. 7 Applications of rotating magnetic field-driven microrobots. (a) Schematic of an artificial sperm-hybrid microrobot that carries drug (reproduced with permission from ref. 112. Copyright 2018, American Chemical Society). (b) Schematic and microscope images of a helical microrobot with nanostructures for easy observation (reproduced with permission from ref. 118. Copyright 2020, John Wiley & Sons, Inc.). (c) Schematic illustration of multiple manipulation modes performed by a microswimmer, which can be used as a manipulator to push and move objects (reproduced with permission from ref. 119. Copyright 2014, Royal Society of Chemistry). (d) Schematic and microscope images of particle transportation achieved by a syringe-like microrobot (reproduced with permission from ref. 120. Copyright 2015, John Wiley & Sons, Inc.). (e) Schematic of object transportation performed by a swarm of spherical microrobots (reproduced with permission from ref. 124. Copyright 2019, American Association for the Advancement of Science).

field. Apart from individual microrobots, a rotating magnetic field can also be used to control and actuate a microrobot swarm.[121–125] As shown in Fig. 7(e),[124] peanut-shaped microrobots were developed, which are made of 3-methacryloxypropyl trimethoxysilane (TPM) and hematite cubes. When placed in a rotating magnetic field, the magnetic microrobot swarm can change its shape and mechanical layout on demand to pass through narrow channels and actuate large payloads. The microrobot swarm is capable of transforming and reshaping mechanical structures, which are useful for multitasking and working in different environments.

Microrobots driven by rotating magnetic fields (also known as torque-driven microrobots) can effectively move and translate in fluidic environments with low Reynolds numbers. Despite the aforementioned advantages and useful applications, several limitations still exist for this type of microrobot, especially in designing magnetic control systems. Using rotating magnets to generate a rotating magnetic field is a straightforward and easy method to generate a magnetic field in a small area with strong field strength. However, it is difficult to use this method to achieve precise control and actuation of the microrobot as the magnetic field generated by this method is highly nonlinear and distorted. Electromagnetic coils are also widely used to generate rotating magnetic fields, and the field strength and distribution can be easily adjusted by controlling the electric current running through the coils. However, such coils are complex and expensive to build, and it is difficult to build a system that can create strong magnetic fields inside a small working area. There are many different magnetic-torque-driven microrobots developed and used for different applications. However, the underlying actuation mechanisms for a majority of them are still unclear due to complex interactions of these microrobots with different physical fields. It is expected that future research in this area will

focus on the improvement of magnetic control systems to achieve efficient and precise manipulation of microrobots and the development of simulation models to understand the physical mechanisms that determine their moving behaviors under different experimental conditions.

Microrobots driven by magnetic field gradient. Magnetic field gradient-driven microrobots are actuated by magnetic gradient force, which can be expressed as:

$$F_m = V(M\cdot\nabla)B \quad (2)$$

in which V [m^3] represents the volume of the magnetic object, M [A m^1] represents the magnetization of the magnetic object and B [T] represents the magnetic field. They align themselves with the direction of the magnetic field and move in the direction of the field gradient.[126–130] The actuation mechanism is shown in Fig. 8(a). Compared with microrobots actuated by a rotating magnetic field or an alternating magnetic field, the microrobots driven by magnetic field gradients have little restrictions on mechanical structures and can move along the direction of the field gradient. Spherical and cylindrical structures are widely used for magnetic field gradient-driven microrobots because such structures experience little surface frictional force, as shown in Fig. 8(b). These microrobots are mainly fabricated using electrodeposition, UV polymerization and micromolding.[131–139] They can easily achieve long-distance locomotion and precise payload delivery,[101,102] thus suitable for many biomedical applications.

Fig. 9(a)–(e) show examples of using a magnetic field gradient to drive microrobots for cargo transport and drug delivery. Fig. 9(a) shows a burr-like porous spherical microrobot fabricated using 3D laser lithography.[131] The microrobot was coated with Ni to enable magnetic actuation and Ti to ensure biocompatibility. Under magnetic field gradient actuation, the microrobot can automatically navigate in zebrafish embryos. Moreover, the microrobot can also move freely and release HeLa cells inside a mouse body. The above results demonstrate the feasibility of using burr-like microrobots for targeted cell delivery *in vivo*. In this work, the magnetic microrobot is biocompatible instead of biodegradable. For *in vivo* applications, it is important to develop fully biodegradable microrobots to minimize potential harmful effects. Fig. 9(b) shows a superhydrophilic magnetic iron bead, which was placed inside a water droplet and functions as a microrobot.[132] Driven by an external magnet, the microrobot together with the droplet can move freely in 3D space to cross over physical barriers for payload transportation. In this work, a single magnet was used to actuate a single droplet. However, it is expected that parallel control of multiple droplets is possible with a multiple-magnet-based control system.

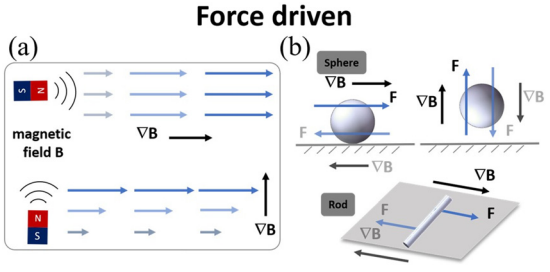

Fig. 8 (a) Schematic of magnetic field gradient actuation. (b) The typical models of magnetic field gradient-driven microrobots (sphere and rod).

Relying on the force generated by a magnetic field gradient, microrobots can be used to capture payload, transport it to the desired site and release the payload on demand.[133–136] As shown in Fig. 9(c), a microrobotic gripper was actuated by a magnetic field gradient to clamp and transport targeted objects.[137] To fabricate the microgripper, a mixture of polyurethane and magnetic particles (ferrite and NdFeB) was first injected into a micro-mold and then polymerized using UV light. After the fabrication, the microgripper was placed in an electromagnetic system. By adjusting the magnetic field strength or using a pulsed magnetic field, the microgripper can achieve stick-slick locomotion and 3D motion and precisely capture targets with a wide size range. In this work, the microgripper is mainly used to achieve long-distance target transportation and 3D assembly. Fig. 9(d) shows a shape-morphing starfish-like magnetic microrobot fabricated using microelectrodes and photoresist.[138] The photoresist was first filled into the gap between the two electrode plates. By applying an electric field between the two plates, the photoresist can be electrically polymerized to form the mechanical structure of the microrobot. This microrobot is mainly made of soft materials and can change its shape to catch and release objects in response to different ion levels. These unique features make the microrobot capable of capturing, transporting and releasing cells, which may be useful for disease diagnosis and medical therapy *in vivo*. Apart from controlling single microrobots, magnetic field gradients can also be used to control microswarms. Fig. 9(e) shows the use of a magnetic microswarm for active endovascular drug delivery.[139] To actuate the microswarm, a magnet fixed on an *XY* stage is used to generate gradient force that can drag the microswarm. By moving the magnet, the microswarm can be moved to desired sites and positions. After using ultrasound Doppler imaging, the microswarm can be visualized and guided to work in blood vessels. More importantly, the microswarm can withstand blood flow and keep its position after applying the magnetic field. This approach of joint use of a microrobotic swarm and advanced medical imaging techniques enables precise drug delivery in blood vascular systems.

Although magnetic field gradients can be used to drive and manipulate microrobots for a variety of applications, several challenges still remain. For example, it is still unknown whether it is safe to use these microrobots for *in vivo* biomedical applications. In addition, the magnetic field gradient-driven microrobots can move fast in a

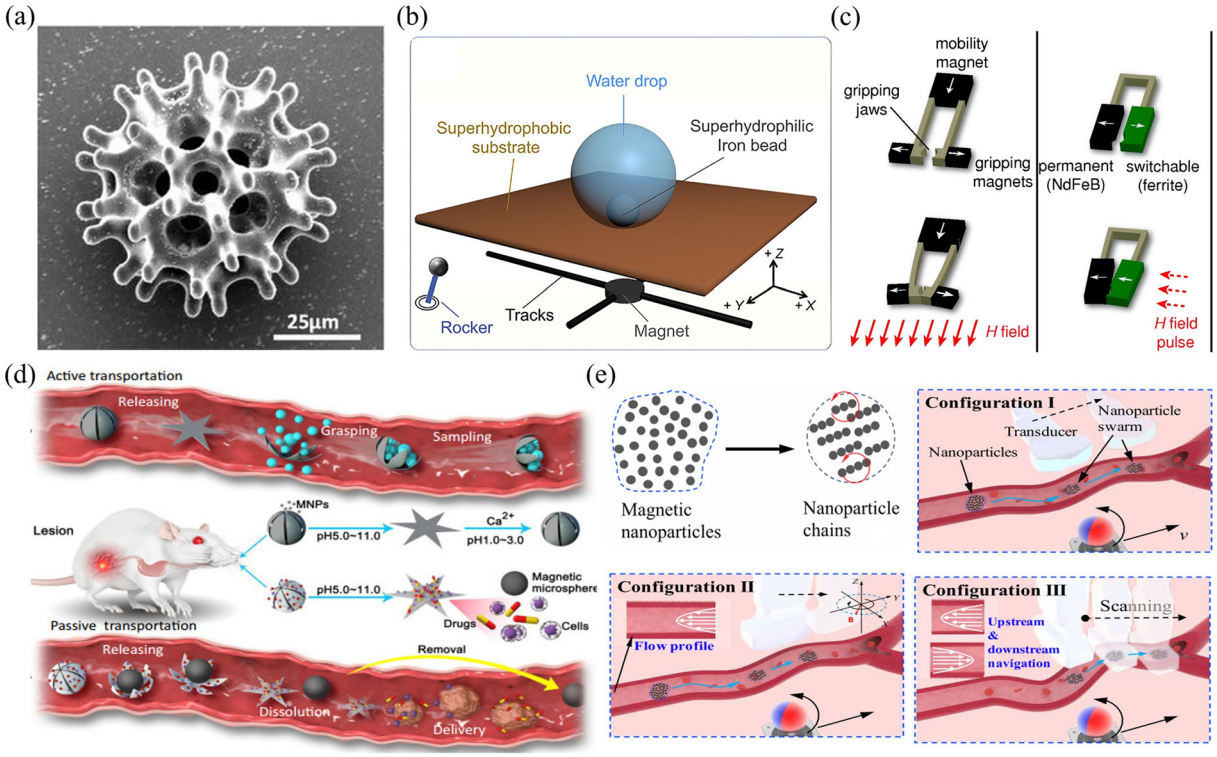

Fig. 9 Applications of magnetic field gradient-driven microrobots. (a) Scanning electron microscope image of a burr-like porous spherical microrobot (reproduced with permission from ref. 131. Copyright 2018, American Association for the Advancement of Science). (b) The locomotion mechanism of a microbead sitting on a superhydrophobic interface (reproduced with permission from ref. 132. Copyright 2021, Elsevier). (c) The mechanism of grasping motion performed by a microgripper (reproduced with permission from ref. 137. Copyright 2014, John Wiley & Sons, Inc.). (d) The mechanism of passive and active object delivery performed by a shape-morphing starfish-like microrobot (reproduced with permission from ref. 138. Copyright 2021, Nature Publishing Group). (e) Schematic of intravascular therapy based on ultrasonic guidance and magnetic actuation of nanoparticles (reproduced with permission from ref. 139. Copyright 2021, American Association for the Advancement of Science.)

magnetic field with a large field gradient, but their mobility is significantly reduced in environments with a small field gradient. Future research in this area will focus on the development of useful strategies to control magnetic field gradients in 3D. This will allow microrobots to achieve more complex and useful locomotion in 3D and will also be useful for applications requiring high manipulation precision such as single-cell therapy and gene transfection. In addition, it is believed that new microrobotic designs such as mini vehicles, valve-type swimmers, and multiarmed clamps will play an important role in improving the performance of magnetic field gradient-driven microrobots in the future.

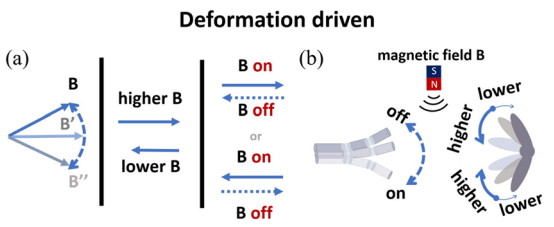

Fig. 10 (a) Schematic of alternating magnetic field actuation. (b) The typical models of alternating magnetic field-driven microrobots are shape-deformable and multi-component structures.

Microrobots driven by alternating magnetic fields. Alternating magnetic fields are magnetic fields whose strength or direction changes periodically, as shown in Fig. 10(a). The periodic change of the magnetic field is characterized by a field vector, which can be expressed as:

$$B(f, t) = B[|\cos(2\pi ft)|n + \sin(2\pi t)u] \quad (3)$$

in which n and u are the orthogonal unit vectors in the plane. M [A m^1] represents the magnetization of magnetic objects and B [T] represents the magnetic field. Compared with the microrobots actuated by a rotating magnetic field or magnetic field gradients, the microrobots driven by alternating magnetic fields rely on asymmetrical shape deformation to escape Purcell's famous "scallop theorem".[140] The most common structure of alternating magnetic field-driven microrobots is a multijoint structure, which is inspired by the swimming mechanism of fish or bacterial flagellum,[141–145] as shown in Fig. 10(b). Fabrication methods such as self-assembly, electrodeposition and template-based printing are widely used to fabricate alternating magnetic field-driven microrobots.[146–149] Fig. 11(a) shows a fish-like body-deformable biomimetic microswimmer fabricated using electrodeposition.[150] The artificial microrobot consists of one

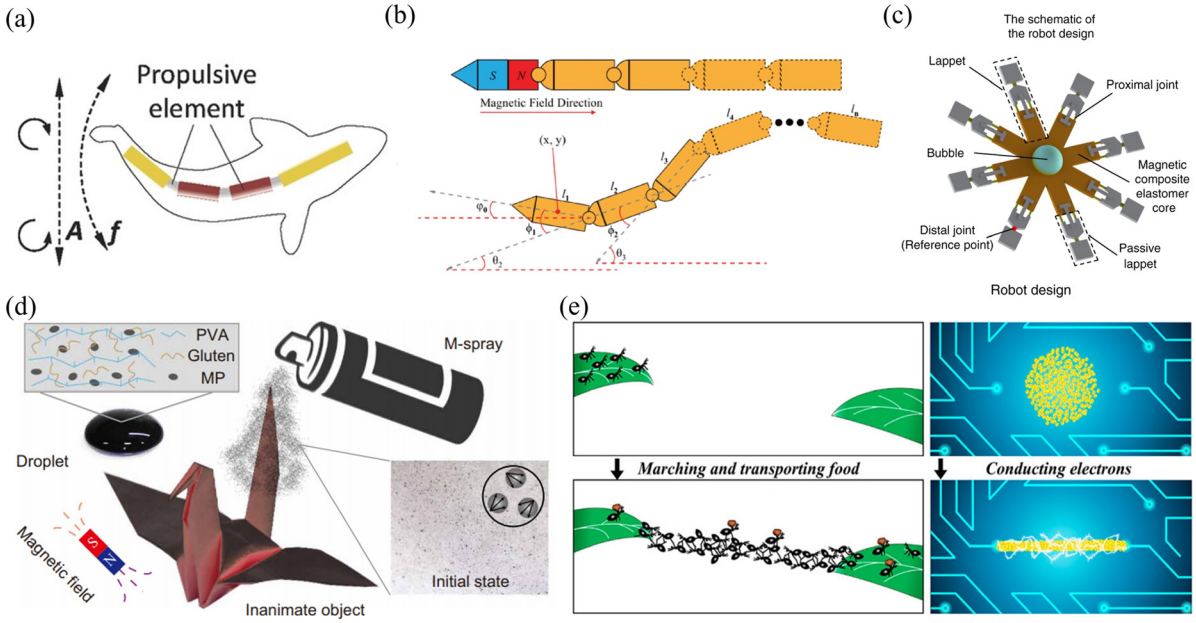

Fig. 11 Applications of alternating magnetic field-driven microrobots. (a) Schematic of propulsion performed by a fish-like microrobot that was actuated under an on–off magnetic field (reproduced with permission from ref. 150. Copyright 2016, John Wiley & Sons, Inc.). (b) The motion mechanism of a snake-like microrobot, which can achieve efficient movement in a fluidic environment (reproduced with permission from ref. 151. Copyright 2021, IEEE). (c) Schematic of multiple motion modes performed by a jellyfish-like microrobot, which can clamp or grasp a microbead and transport it to other sites (reproduced with permission from ref. 152. Copyright 2019, Nature Publishing Group). (d) Schematic of a shape-deformable crane-like microrobot working in a magnetic field (reproduced with permission from ref. 107 Copyright 2020, American Association for the Advancement of Science). (e) Schematic of using a swarm of magnetic nanoparticles to build an electric circuit (reproduced with permission from ref. 158. Copyright 2019, American Chemical Society).

gold segment as the head, two nickel segments as the body, and one gold segment as the caudal fin. The three parts were connected by three flexible silver hinges. After applying an oscillating magnetic field, the microrobot was tested for swimming behaviour and the results were used to optimize the segment length of the microrobot. Similar to the fish-like microrobot, a multi-segment snake-like microswimmer was also developed, as shown in Fig. 11(b).[151] Its body was fabricated using two-photon photolithography and its head segment was deposited with a thin layer of Ni. This work used many theoretical analyses and experiments to demonstrate that the microrobot required a minimum of three segments to move forward smoothly and required more segments (four, five is the maximum) to achieve good moving performance. These results inspired researchers to investigate the driving mechanism and motion performance of microrobots made of multiple segments. It is expected that such microrobots will also inspire ideas to design new microrobots with applications for micromanipulation and microfabrication.

Magnetic fields can change with time and space, allowing microrobots to move in different modes for different applications. Fig. 11(c) shows a jellyfish-like soft microrobot fabricated using the bio-templating method.[152] When placed in an oscillating magnetic field, the microrobot can be used to capture and transport targeted objects, burrow and search targets, and mix fluids. This microrobot can move in different locomotion modes without being influenced by physiological factors, providing an ideal scientific tool to mimic and study the moving behaviours of ephyrae. Such microrobots are useful for biomedical research and environmental study. Fig. 11(d) shows another multi-component crane-like microrobot which was inspired by origami. To fabricate this kind of microrobot, a cured PDMS film was folded and its surface was sprayed with agglutinate magnetic film.[107] When placed in an oscillating magnetic field, the microrobot can be actuated and used to carry payloads. The unique design also enables this microrobot to transform its shape and perform different movements, such as 'flapping', 'hovering', 'turning' and 'side-slipping'. This origami-inspired microrobot can easily change its shape and mechanical structure to adapt different applications or working conditions. In addition to origami-inspired microrobots, alternating magnetic field-driven microrobotic swarms are reconfigurable as well and often used for large-scale cargo transportation, object gathering and microassembly.[153–157] Fig. 11(e) shows a microswarm actuated by oscillating magnetic fields.[158] The microrobotic swarm consists of Fe_3O_4 nanoparticles coated with a thin Au layer. The microrobotic swarm is conductive and can be effectively actuated by an oscillating magnetic field. These microrobotic swarms can be used in many microelectronic experiments, such as forming conductive microstructures to light up LED arrays and bridge broken electrodes. In addition to superior magnetic and electrical properties, these microrobotic swarms can be functionalized with other properties to mimic collective behaviours of living systems.

Although several studies of alternating magnetic field-driven microrobots have proven that they can be used in low Reynolds number fluid environments, they still face challenges for use *in vivo* such as in flowing blood vessels. In the future, researchers should consider combined control strategies, including spatial oscillation, rotation and gradient field, which can be utilized to improve the effectiveness of time-asymmetric actuation. Additionally, the surface functionalization of microrobots and the interaction between microrobots and the surrounding fluid are important factors that need to be considered when the microrobots are used for *in vivo* applications.

Commercialization of magnetic microrobot systems

Although holding great potential for different applications, magnetic microrobots are still at the very early stage for commercialization. In contrast, magnetic actuation systems are relatively mature in the biomedical field and used for a variety of applications such as endovascular therapy, gastrointestinal inspection, and cardiothoracic surgery.[159] The Niobe robotic magnetic actuation system (Stereotaxis Inc., MO, USA) is one such example, which can be used to control magnetic catheters to perform minimally invasive cardiovascular surgery.[160] As shown in Fig. 12(a), the system consists of two strong rotatable permanent magnets located at the side of the patient's bed, which can provide a controllable magnetic field to operate the catheters. To date, the Niobe system has been used to treat more than 100 000 patients globally.

Another example of a magnetic actuation system for biomedical applications is magnetic resonance imaging (MRI), which is a powerful imaging tool for diagnosis.[161] The MRI instrument consists of two orthogonal Golay coils and a Maxwell coil. The three coils can be used together to generate a strong uniform magnetic field in the horizontal plane and a constantly changing magnetic field with a large field gradient in 3D space, as shown in Fig. 12(b). MRI can be used for both imaging and actuation, providing a useful scientific tool for medical research.

Electromagnets are also used to develop magnetic actuation systems for cardiovascular surgery.[162] In these systems, multiple electromagnets are positioned around the workspace to focus the magnetic field onto the target. Fig. 12(c) shows an image of the Catheter Guidance Control and Imaging (CGCI) system developed by Magnetecs Corporation (California, USA). This system consists of eight electromagnets,[162] with four of them semispherically arranged above the torso, and the rest of them placed symmetrically below the torso. The system is primarily used for magnetic catheter steering with applications in interventional cardiology, gastroenterology and neurology.

The number of people suffering from vascular diseases is expected to increase significantly over the next few decades due to the aging population and growing rate of obesity. There is a strong demand to develop useful tools for vascular interventions. Magnetically actuated interventional instruments are precise, efficient and reliable for cardiothoracic surgery with the advantages of being minimally invasive and compatible with many imaging techniques. A lot of efforts have been put to improve magnetic actuation systems for medical applications and it is expected that such systems will play an increasingly important role in future healthcare systems.

Comparisons of optical and magnetic field-driven microrobots

Similarities. From the view of the actuation mechanism, both optical microrobots and magnetic microrobots are actuated by physical field sources and convert the external potential energy into kinetic energy. Optical field-driven microrobots can acquire power from the light pressure of the laser or the optical gradient force induced by the laser to achieve locomotion. They can be actuated by a single beam, multiple beams or even light patterns, which are accessible from different light sources, including lasers, LEDs, and DMDs.[22,23,27,28,62,73,75,77] Magnetic field-driven microrobots can receive torque or force generated by changes in the external magnetic field for navigation or transportation. They can be actuated by permanent magnets,[163–165] electromagnetic coils,[166–168] or other different configurations of magnetic devices.[169–172] Moreover, both optical microrobots and magnetic microrobots need imaging equipment (*e.g.*, microscope, high-resolution camera), computers, and a user interface to

Fig. 12 Commercial magnetic actuation equipment for healthcare applications. (a) Image of the Niobe system (reproduced with permission from ref. 160. Copyright 2007, John Wiley & Sons, Inc.). (b) Image of the MRI system (reproduced with permission from ref. 161. Copyright 2017, IEEE). (c) Image of the CGCI system (reproduced with permission from ref. 162. Copyright 2010, Radcliffe Medical Media).

be controlled in given applications. Because of the small feature sizes, optical microrobots and magnetic microrobots are mainly fabricated using photolithography, two-photon polymerization, micromolding, metal deposition and other microfabrication techniques. The functions of optical microrobots and magnetic microrobots include micromanipulation, micro-assembly, micro-characterization and cargo transportation. They are mainly used for physics, chemistry, and, in particular, biomedical engineering research. Optical microrobots and magnetic microrobots can interact with a variety of objects including micro-/nanoparticles, electronic/photonic components, cells and microtissues. In addition, most optical and magnetic microrobots are required to work in a liquid environment so that forces from an external field can be effectively exerted on them to provide the driving force.

Differences. In terms of structural design and actuation methods, there are many differences between optical and magnetic field-driven microrobots. Optical microrobots can be designed in a variety of structures and made of different materials. Light force can be exerted on the whole body or individual parts of the microrobot to make it move. OT and OET are typical methods used to drive optical microrobots. Both techniques allow parallel and independent control of multiple microrobots simultaneously by projecting multiple light beams or light patterns. Magnetic microrobots require magnetic-responsive materials used in the fabrication process, including those coated on the microrobot surface or encapsulated inside the microrobot body.[105,138] Moreover, magnetic microrobots need to be magnetized to ensure that the magnetization of the body is aligned with the direction of the external magnetic field. If a magnetic microrobot consists of multiple units, each unit should be magnetized in different directions to ensure the capability of the microrobot to move in different modes. A rotating magnetic field is usually utilized to actuate rotator-type microrobots and make them show rolling motions or corkscrew motions.[115,117] A magnetic field gradient is utilized to draw or push a microrobot body moving in a line (along the direction of the field gradient) and keep its whole body or a part of its structure in a fixed posture, such as a microgripper or microtransporter.[135,137] Alternating magnetic fields combine the features of a rotating magnetic field and magnetic gradient field, which can actuate soft microrobots or microrobots with flexible components based on asymmetric reciprocating motions or undulatory motions.[150,151] Optical actuation has a limited manipulation area which the light must reach, and the light pathway should not be blocked. Magnetic actuation has a relatively large operation area and can control objects to move in 2D or 3D space. For some *in vivo* biomedical applications, magnetic actuation is easier to apply than optical actuation due to larger field penetration depth. Moreover, both optical actuation and magnetic actuation have limited force output depending on the structural scale of the body and actuation parameters of the power system. However, magnetic actuation normally can exert a stronger manipulation force and create a higher moving speed due to the simplicity to generate a relatively stronger magnetic field or increase the magnetic response of the microrobots.

Pros and cons. Optical and magnetic field-driven microrobots have their own characteristics as reported above, and we have summarized their pros and cons in Table 1. Optical tweezers (OT) can precisely trap a single object and exert manipulation force. However, it is challenging to exert strong manipulation force *via* OT, which sets limitations to the size, structures and applications of the microrobots. Optoelectronic tweezers (OET) can generate light-induced DEP force to control microrobots based on light patterns instead of light beams. OET allows easy control of multiple microrobots simultaneously and is capable of exerting stronger force to drive larger microrobots. However, OET relies on the use of photoconductive materials which are normally fabricated

Table 1 Comparison of pros and cons between optical field-driven microrobots and magnetic field-driven microrobots

Actuation source	Types of field-driven microrobots	Characteristics and advantages	Limitations
Optical stimuli	Optical tweezers (OT)	High precision of manipulation[22,23] Single-beam or multiple-beams[56,57]	Small actuation force[37–42] Require finely controlled optical parameters[22–26] Require the pathway of light unblocked
	Optoelectronic tweezers (OET)	Parallel control and actuation[75,77,78] Stronger manipulation force[82]	Require photoconductive materials[75,77–84]
	Heat-mediated optical manipulation	Non-contact manipulation Bubble-based microrobot[96–98]	Low precision of manipulation[97,98]
Magnetic stimuli	Rotating magnetic field	High efficiency of locomotion and transportation[120,121] Flexible steering[105,113,118]	Simple structure[114–116] Require a complex control system[108,111,112]
	Magnetic field gradient	High-precision manipulation[138] Strong manipulation force[137] Linear movement[132]	Uniform manipulation force[129,130] Limited to 2D manipulation[139]
	Alternating magnetic field	Flexible and multifunctional motions[107,150] Suitable for viscous environment[152]	Require ingenious structural design[151] Require complex control strategies[143,147,158]

using expensive semiconductor fabrication tools in cleanroom settings that are not easily accessible to many end users. Optical-heating microrobots utilize optical thermal gradient force. In some cases, optical thermal effects can be utilized to generate microbubbles in fluid, which can be used as microrobots to move secondary objects. Normally, it requires a specific substrate that can effectively convert light into heat to generate microbubble-based microrobots. In addition, it requires precise control of the optical power to adjust the physical properties of the microbubble, and the manipulation precision of the microbubble-based microrobot is not as high as those controlled by OT and OET. Due to the properties of light, it is difficult to achieve precise manipulation of optical microrobots *in vivo* so most optical microrobots are used for *in vitro* applications. Most light sources for OT and OET are biofriendly and easily work with biological samples. However, strong light intensity over biological samples may create thermal damage and result in phototoxicity.

Rotating magnetic field-driven microrobots, especially those with helical structures, can convert rotation into thrust and move linearly in a fluidic environment. They can swim forward at high speed with little vibration. However, their mechanical structures are relatively fixed, meaning these microrobots may not be suitable for certain applications. Magnetic field gradient-driven microrobots need stronger actuation force than other types of magnetic microrobots to overcome friction from the substrate or the surrounding fluids. Some magnetic field gradient-driven microrobots have the capability to move and individually control different parts of the body. Therefore, they can be used to do a variety of complex mechanical work, such as gripping, holding and releasing. Most alternating magnetic field-driven microrobots have a soft and flexible body. The microrobots can make reversible mechanical changes in the body to generate actuation force and move in viscous fluidic environments. However, their moving velocity is small and the motion is not smooth. In addition, some mechanical motions, such as paddling, flapping, mixing, and shaking, require complex control strategies and result in an increase in the system complexity.

Overall, optical field-driven microrobots are suitable for precise manipulation but need an environment that light can go through. The number of controlled microrobots should be single or a limited number to ensure better manipulation performance. Magnetic field-driven microrobots are more suitable for *in vivo* applications compared with optical microrobots due to the deeper penetration depth of the

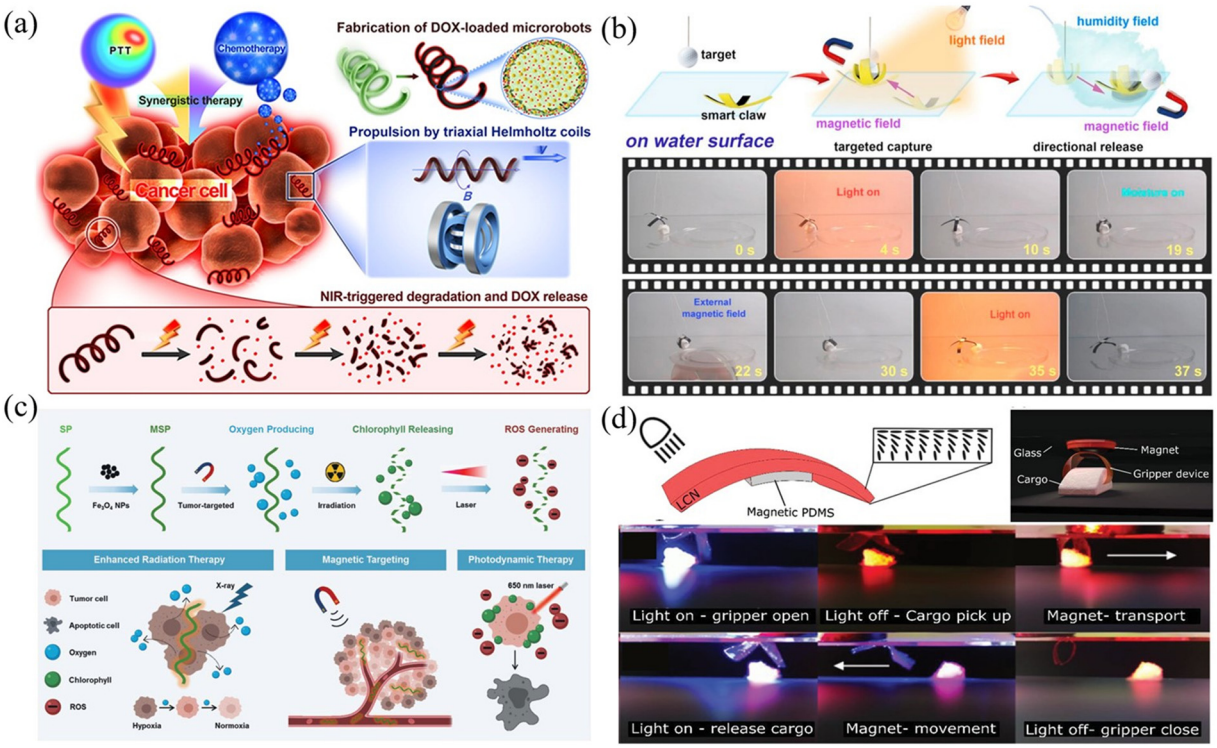

Fig. 13 Joint use of optical and magnetic fields in microrobot actuation. (a) Schematic of propulsion, NIR-triggered degradation, DOX release, and chemo-photothermal treatment toward cancer cells using microrobots (reproduced with permission from ref. 178. Copyright 2019, American Chemical Society). (b) A helical microrobot can respond to dual stimuli of optical and magnetic fields and show multiple functions (reproduced with permission from ref. 179. Copyright 2020, Elsevier Inc). (c) Schematic of magnetic-responsive multifunctional microrobots capable of performing radiation therapy and photodynamic therapy (reproduced with permission from ref. 180. Copyright 2020, John Wiley & Sons, Inc.). (d) Images of the microgripper actuated by light and magnetic field to perform a series of movements including rotating, grasping, walking, holding, and releasing (reproduced with permission from ref. 181. Copyright 2019, John Wiley & Sons, Inc.).

magnetic field in the body. Moreover, magnetic actuation can control microrobots in a swarm to show high efficiency in translation or manipulation. However, magnetic microrobots require magnetic materials to be encapsulated into the structure or coated on the surface; thus, the problem of toxic residues needs to be carefully considered when used for *in vivo* biomedical applications.

Joint use of optical and magnetic field actuation in microrobots

The joint use of optical and magnetic field-driven microrobots provides an interesting approach for many applications. As demonstrated above, magnetic field-driven microrobots are useful for many biomedical applications, such as intracellular manipulation, microsurgery, and drug delivery, and provide a promising platform for simulating and studying the physics of active matter.[173–177] Fig. 13(a) shows biohybrid magnetic microrobots (BMMRs) that are used for targeted delivery and synergistic chemo-photothermal therapy.[178] The obtained microrobots can be actuated in an external magnetic field to achieve drug delivery and perform synergistic chemo-photothermal therapy to kill EC109 and 769-P cancer cells upon an 808 NIR laser irradiation. More importantly, the biohybrid microrobots can degrade under NIR irradiation and release drugs to the nearby environment. This work provides an integrated strategy for fabricating multifunctional microrobots with high swimming speed, precise directional guidance, ultrahigh drug loading efficiency as well as efficient photothermal conversion capability toward applications of targeted drug delivery and synergistic chemo-photothermal therapy in a single microrobotic platform. Fig. 13(b) shows a photosynthetic biohybrid nanoswimmer (PBN) system-based on magnetically engineered bacteria, *Spirulina platensis*. The PBNs can be utilized for tumor-targeted imaging and therapy.[179] The engineered PBNs were fabricated using superparamagnetic magnetite (Fe_3O_4 NPs) *via* a dip-coating process, enabling their tumor targeting ability and magnetic resonance imaging properties after intravenous injection. PBNs can be used as oxygenators for *in situ* O_2 generation in hypoxic solid tumours through photosynthesis, modulating the tumour microenvironment (TME), and thus improving the effectiveness of radiotherapy (RT). Furthermore, the innate chlorophyll released from the RT-treated PBNs, as a photosensitizer, can produce cytotoxic reactive oxygen species under laser irradiation to achieve photodynamic therapy. This work provides a novel platform for achieving tumour-specific enhanced combination therapy under the guidance of FL (fluorescence)/PA (photoacoustic)/MR (magnetic resonance) imaging. As shown in Fig. 13(c), another kind of microrobot was made from multi-responsive materials.[180] The microrobot is made of dual-responsive soft materials and can be remotely actuated using both magnetism and light. The multiform stimulations can coordinate with each other, which enables the microrobot to perform integrated complex motions such as translating, bending, gripping, releasing and rotating. Fig. 13(d) shows a dual magneto and photoresponsive soft robotic microgripper, capable of loading, transporting, rotating, and releasing cargo.[181] This microgripper mainly consists of a light-responsive LCP thin film coated with a magnetically responsive layer. Light is used to trigger the mechanical changes of the microgripper, making it grab, pick up and release cargo with a high degree of control. Magnetic control is employed to conduct the translation and rotation of the microgripper. These examples demonstrated the combined use of optical and magnetic fields for microrobotic research and the related applications in medical therapy, drug delivery and micromanipulation. Because of the complementary and compatible nature of optical and magnetic actuation techniques, it is expected that the joint use of the two techniques will become more and more important in future microrobotic research.[182,183]

Summary

This paper presents a comprehensive review of microrobots driven by optical and magnetic fields, including their design, actuation mechanisms and related applications. For microrobots driven by optical fields, we summarized the use of optical tweezers, optoelectronic tweezers, and heat-mediated optical manipulation techniques to drive microrobots. For microrobots driven by magnetic fields, we summarized the use of rotating magnetic fields, magnetic gradient fields, and alternating magnetic fields to drive microrobots. Then we compared the similarities and differences between the two types of field-driven microrobots and discussed their advantages and disadvantages. Finally, we presented recent advances in the joint use of optical and magnetic field actuation of microrobots. With the rapid development of new materials, fabrication technologies, and actuation strategies and due to great efforts to improve microrobot technology by researchers worldwide, we believe that research on optical and magnetic field-driven microrobots will continue to thrive in the near future and will play an increasingly important role in physics, chemistry and, in particular, biomedical engineering.

Conflicts of interest

There are no conflicts to declare.

Acknowledgements

This work is supported by the National Key R&D Program of China under grant number 2019YFB1309701 and the National Natural Science Foundation of China under grant number 62073042, 62088101, 62103050 and 62105177.

References

1 M. Z. Miskin, A. J. Cortese and K. Dorsey, *Nature*, 2020, **584**, 557–561.

2 B. H. Kim, K. Li and J. T. Kim, *Nature*, 2021, **597**, 503–510.
3 S. Palagi and P. Fischer, *Nat. Rev. Mater.*, 2018, **3**, 113–124.
4 P. Fischer and B. J. Nelson, *Sci. Robot.*, 2021, **6**, eabh3168.
5 H. Ceylan, J. Giltinan, K. Kozielski and M. Sitti, *Lab Chip*, 2017, **17**, 1705–1724.
6 C. K. Schmidt, M. Medina-Sánchez, R. J. Edmondson and O. G. Schmidt, *Nat. Commun.*, 2020, **11**, 5618.
7 S. Jeon, S. Kim, S. Ha, S. Lee, E. Kim, S. Y. Kim, S. H. Park, J. H. Jeon, S. W. Kim, C. Moon, B. J. Nelson, J. Kim, S.-W. Yu and H. Choi, *Sci. Robot.*, 2019, **4**, eaav4317.
8 S. Tottori, L. Zhang, F. Qiu, K. K. Krawczyk, A. Franco-Obregón and B. J. Nelson, *Adv. Mater.*, 2012, **24**, 811–816.
9 Y. Alapan, B. Yigit, O. Beker, A. F. Demirörs and M. Sitti, *Nat. Mater.*, 2019, **18**, 1244–1251.
10 J. Yu, B. Wang, X. Du, Q. Wang and L. Zhang, *Nat. Commun.*, 2018, **9**, 3260.
11 H. Xie, X. Fan, M. Sun, Z. Lin, Q. He and L. Sun, *IEEE ASME Trans. Mechatron.*, 2019, **24**, 902–912.
12 X. Wang, X. Z. Chen, C. C. J. Alcântara, S. Sevim, M. Hoop and A. Terzopoulou, *Adv. Mater.*, 2019, **31**, 1901592.
13 T. Xu, C. Huang, Z. Lai and X. Wu, *IEEE Trans. Robot.*, 2022, **38**, 2875–2887.
14 C. W. Shields IV, K. Han, F. Ma, T. Miloh, G. Yossifon and O. D. Velev, *Adv. Funct. Mater.*, 2018, **28**, 1803465.
15 X. Xu, C. Liu, K. Kim and D. L. Fan, *Adv. Funct. Mater.*, 2014, **24**, 4843–4850.
16 K. Kim, X. Xu and J. Guo, *et al.*, *Nat. Commun.*, 2014, **5**, 3632.
17 J. H. Guo, J. J. Gallegos, A. R. Tom and D. L. Fan, *ACS Nano*, 2018, **12**, 1179–1187.
18 M. Kaynak, A. Ozcelik, A. Nourhani, P. E. Lammert, V. H. Crespi and T. J. Huang, *Lab Chip*, 2017, **17**, 395–400.
19 A. Aghakhani, A. Pena-Francesch, U. Bozuyuk, H. Cetin, P. Wrede and M. Sitti, *Sci. Adv.*, 2022, **8**, eabm5126.
20 M. Kaynak, A. Ozcelik, N. Nama, A. Nourhani, P. E. Lammert, V. H. Crespi and T. J. Huang, *Lab Chip*, 2016, **16**, 3532–3537.
21 A. Aghakhani, O. Yasa, P. Wrede and M. Sitti, *Proc. Natl. Acad. Sci. U. S. A.*, 2020, **117**, 3469–3477.
22 D. Palima and J. Glückstad, *Laser Photonics Rev.*, 2013, **7**, 478–494.
23 A. I. Bunea and J. Glückstad, *Laser Photonics Rev.*, 2019, **13**, 1800227.
24 T. Asavei, T. A. Nieminen, V. L. Y. Loke, A. B. Stilgoe, R. Bowman, D. Preece, M. J. Padgett, N. R. Heckenberg and H. Rubinsztein-Dunlop, *New J. Phys.*, 2013, **15**, 063016.
25 S. Maruo, A. Takaura and Y. Saito, *Opt. Express*, 2009, **17**, 18525–18532.
26 N. K. Metzger, M. Mazilu, L. Kelemen, P. Ormos and K. Dholakia, *J. Opt.*, 2011, **13**, 044018.
27 A. Ashkin, J. M. Dziedzic, J. E. Bjorkholm and S. Chu, *Opt. Lett.*, 1986, **11**, 288–290.
28 A. Ashkin, J. M. Dziedzic and T. Yamane, *Nature*, 1987, **330**, 769–771.
29 P. H. Jones, O. M. Maragò and G. Volpe, *Optical Tweezers: Principles and Applications*, Cambridge University Press, 2015.
30 L. Zhang, K. E. Peter and B. J. Nelson, *Lab Chip*, 2010, **10**, 2203–2215.
31 W. Hu, G. Z. Lum, M. Mastrangeli and M. Sitti, *Nature*, 2018, **554**, 81–85.
32 A. Li, H. Li, Z. Li, Z. Zhao, K. Li, M. Li and Y. Song, *Sci. Adv.*, 2020, **6**, eaay5808.
33 H. Y. Zhang, Z. Z. Li, C. Y. Gao, X. J. Fan, Y. X. Pang, T.-L. Li, Z.-G. Wu, H. Xie and Q. He, *Sci. Robot.*, 2021, **6**, eaaz9519.
34 Z. Wu, Y. Chen, D. Mukasa, O. S. Pak and W. Gao, *Chem. Soc. Rev.*, 2020, **49**, 8088–8112.
35 A. Aziz, S. Pane, V. Iacovacci, A. Menciassi, M. Medina-Sánchez and O. G. Schmidt, *ACS Nano*, 2020, **14**, 10865–10893.
36 P. Wang, M. A. R. Al Azad, X. Yang, P. R. Martelli, K. Y. Cheung, J. Shi and Y. J. Shen, *Proc. Natl. Acad. Sci. U. S. A.*, 2021, **118**, e2024329118.
37 H. Zeng, D. Martella, P. Wasylczyk, G. Cerretti, J. C. Lavocat, C. H. Ho, C. Parmeggiani and D. S. Wiersma, *Adv. Mater.*, 2014, **26**, 2319–2322.
38 S. Palagi, A. G. Mark, S. Y. Reigh, K. Melde, T. Qiu, H. Zeng, C. Parmeggiani, D. Martella, A. Sanchez-Castillo, N. Kapernaum, F. Giesselmann, D. S. Wiersma, E. Lauga and P. Fischer, *Nat. Mater.*, 2016, **15**, 647–653.
39 J. Lv, Y. Liu, J. Wei, E. Chen, L. Qin and Y. Yu, *Nature*, 2016, **537**, 179–184.
40 H. Zeng, P. Wasylczyk, D. S. Wiersma and A. Priimagi, *Adv. Mater.*, 2018, **30**, 1703554.
41 M. P. da Cunha, M. G. Debije and A. P. Schenning, *Chem. Soc. Rev.*, 2020, **49**, 6568–6578.
42 S. Palagi, D. P. Singh and P. Fischer, *Adv. Opt. Mater.*, 2019, **7**, 1900370.
43 L. Xu, F. Mou, H. Gong, M. Luo and J. Guan, *Chem. Soc. Rev.*, 2017, **46**, 6905–6926.
44 K. Villa and M. Pumera, *Chem. Soc. Rev.*, 2019, **48**, 4966–4978.
45 A. Ashkin, J. Dziedzic and T. Yamane, *Nature*, 1987, **330**, 769–771.
46 A. Ashkin and J. M. Dziedzic, *Science*, 1987, **235**, 1517–1520.
47 H. Zhang and K. K. Liu, *J. R. Soc., Interface*, 2008, **5**(24), 671–690.
48 M. D. Wang, H. Yin, R. Landick, J. Gelles and S. M. Block, *Biophys. J.*, 1997, **72**, 1335–1346.
49 I. Heller, T. P. Hoekstra, G. A. King, E. J. Peterman and G. J. Wuite, *Chem. Rev.*, 2014, **114**, 3087–3119.
50 F. Nan and Z. Yan, *Angew. Chem., Int. Ed.*, 2019, **58**, 4917–4976.
51 F. Nan, F. Han, N. F. Scherer and Z. Yan, *Adv. Mater.*, 2018, **30**, 1803238.
52 A. Ashkin, *Proc. Natl. Acad. Sci., India, Sect. B*, 1997, **94**, 4853–4860.
53 A. Ashkin, *IEEE J. Sel. Top. Quantum Electron.*, 2000, **6**, 841–856.
54 M. Daly, M. Sergides and S. N. Chormaic, *Laser Photonics Rev.*, 2015, **9**, 309–329.
55 I. A. Favre-Bulle, A. B. Stilgoe, E. K. Scott and H. Rubinsztein-Dunlop, *Nanophotonics*, 2019, **8**, 1023–1040.

56 G. Whyte, G. Gibson, J. Leach, M. Padgett, D. Robert and M. Miles, *Opt. Express*, 2006, **14**, 12497–12502.
57 M. Padgett and R. D. Leonardo, *Lab Chip*, 2011, **11**, 1196–1205.
58 S. L. Neale, M. P. MacDonald, K. Dholakia and T. F. Krauss, *Nat. Mater.*, 2005, **4**, 530–533.
59 T. Wu, T. A. Nieminen, S. Mohanty, J. Miotke, R. L. Meyer, H. Rubinsztein-Dunlop and M. W. Berns, *Nat. Photonics*, 2012, **6**, 62–67.
60 H. Xin, N. Zhao, Y. Wang, X. Zhao, T. Pan, Y. Shi and B. Li, *Nano Lett.*, 2020, **20**, 7177–7185.
61 I. Williams, E. C. Oğuz, T. Speck, P. Bartlett, H. Löwen and C. Patrick, *Nat. Phys.*, 2016, **12**, 98–103.
62 U. G. Būtaitė, G. M. Gibson, Y. L. Ho, M. Taverne, J. M. Taylor and D. B. Phillips, *Nat. Commun.*, 2019, **10**, 1215.
63 X. Zou, Q. Zheng, D. Wu and H. Lei, *Adv. Funct. Mater.*, 2020, **30**, 2002081.
64 D. R. Leonardo, A. Búzás, L. Kelemen, G. Vizsnyiczai, L. Oroszi and P. Ormos, *Phys. Rev. Lett.*, 2012, **109**, 034104.
65 J. Leach, H. Mushfique, R. di Leonardo, M. Padgett and J. Cooper, *Lab Chip*, 2006, **6**, 735–739.
66 S. Bianchi, G. Vizsnyiczai, S. Ferretti, C. Maggi and R. Di Leonardo, *Nat. Commun.*, 2018, **9**, 4476.
67 X. F. Lin, G. Q. Hu, Q. D. Chen, L. G. Niu, Q. S. Li, A. Ostendorf and H. B. Sun, *Appl. Phys. Lett.*, 2012, **101**, 113901.
68 E. Avci, M. Grammatikopoulou and G. Z. Yang, *Adv. Opt. Mater.*, 2017, **5**, 1700031.
69 J. Köhler, S. I. Ksouri, C. Esen and A. Ostendorf, *Microsyst. Nanoeng.*, 2017, **3**, 16083.
70 M. J. Villangca, D. Palima, A. R. Banas and J. Glückstad, *Light: Sci. Appl.*, 2016, **5**, 16148.
71 X. F. Wu, R. E. Ehehalt, G. Razinskas, T. Feichtner, J. Qin and B. Hecht, *Nat. Nanotechnol.*, 2022, **17**, 477–484.
72 Y. Li, X. Liu and B. Li, *Light: Sci. Appl.*, 2019, **8**, 61.
73 D. B. Phillips, M. J. Padgett, S. Hanna, Y. L. Ho, D. M. Carberry, M. J. Miles and S. H. Simpson, *Nat. Photonics*, 2014, **8**, 400–405.
74 D. Palima, A. R. Bañas, G. Vizsnyiczai, L. Kelemen, P. Ormos and J. Glückstad, *Opt. Express*, 2012, **20**, 2004–2014.
75 P. Y. Chiou, A. T. Ohta and M. C. Wu, *Nature*, 2005, **436**, 370–372.
76 S. Zhang, B. Xu, M. Elsayed, F. Nan, W. Liang, J. K. Valley, L. Liu, Q. Huang, M. C. Wu and A. R. Wheeler, *Chem. Soc. Rev.*, 2022, **51**, 9203–9242.
77 M. C. Wu, *Nat. Photonics*, 2011, **5**, 322–324.
78 H. Hwang and J. K. Park, *Lab Chip*, 2011, **11**, 33–47.
79 S. Zhang, W. Li, M. Elsayed, J. Peng, Y. Chen, Y. Zhang, Y. Zhang, M. Shayegannia, W. Dou, T. Wang, Y. Sun, N. P. Kherani, S. L. Neale and A. R. Wheeler, *Small*, 2021, **17**, 2170193.
80 S. Zhang, M. Elsayed, R. Peng, Y. Chen, Y. Zhang, S. L. Neale and A. R. Wheeler, *Photonics Res.*, 2022, **10**, 550–556.
81 S. Zhang, W. Li, M. Elsayed, J. Peng, Y. Chen, Y. Zhang, Y. Zhang, M. Shayegannia, W. Dou, T. Wang, Y. Sun, N. P. Kherani, S. L. Neale and A. R. Wheeler, *Small*, 2021, **17**, 2103702.
82 S. Zhang, E. Y. Scott, J. Singh, Y. Chen, Y. Zhang, M. Elsayed, M. D. Chamberlain, N. Shakiba, K. Adams, S. Yu, C. M. Morshead, P. W. Zandstra and A. R. Wheeler, *Proc. Natl. Acad. Sci. U. S. A.*, 2019, **116**, 14823–14828.
83 S. Zhang, M. Elsayed, R. Peng, Y. J. Chen, Y. F. Zhang, J. X. Peng, W. Z. Li, M. D. Chamberlain, A. Nikitina, S. Y. Yu, X. Y. Liu, S. L. Neale and A. R. Wheeler, *Nat. Commun.*, 2021, **12**, 5349.
84 W. Yang, H. Yu, G. Li, Y. Wang and L. Liu, *Small*, 2017, **13**, 1602769.
85 J. Cui, H. P. Wang, Q. Shi and T. Sun, *Cyborg Bionic Syst.*, 2021, **2021**, 9871396.
86 **https://www.berkeleylights.com/**.
87 S. J. Zost, P. Gilchuk and R. E. Chen, *et al.*, *Nat. Med.*, 2020, **26**, 1422–1427.
88 H. Cho, K. K. Gonzales-Wartz and D. Huang, *et al.*, *Sci. Transl. Med.*, 2021, **13**, eabj5413.
89 K. Le, C. Tan, S. Gupta, T. Guhan, H. Barkhordarian, J. Lull, J. Stevens and T. Munro, *Biotechnol. Prog.*, 2018, **34**, 1438–1446.
90 K. Le, C. Tan, H. Le, J. Tat, E. Zasadzinska, J. Diep, R. Zastrow, C. Chen and J. Stevens, *Biotechnol. J.*, 2020, **15**, 1900247.
91 Y. Bronevetsky, *Cytotherapy*, 2020, **22**, S119.
92 M. Rienzo, K.-C. Lin and K. C. Mobilia, *et al.*, *Lab Chip*, 2021, **15**, 2901–2912.
93 Z. H. Chen, J. Li and Y. B. Zheng, *Chem. Rev.*, 2022, **122**, 3122–3179.
94 F. Liu, Z. Zhang, Y. Wei, Q. Zhang, T. Cheng and X. Wu, *Opt. Express*, 2014, **22**, 23716–23723.
95 D. F. Li, C. Liu, Y. Y. Yang, L. D. Wang and Y. J. Shen, *Light: Sci. Appl.*, 2020, **9**, 84.
96 L. Dai, Z. Ge, N. Jiao and L. Liu, *Small*, 2019, **15**, 1902815.
97 L. Dai, D. Lin, X. Wang, N. Jiao and L. Liu, *ACS Appl. Mater. Interfaces*, 2020, **12**, 57587–57597.
98 W. Hu, K. S. Ishii, Q. Fan and A. T. Ohta, *Lab Chip*, 2012, **12**, 3821–3826.
99 Z. X. Ge, L. Q. Dai, J. H. Zhao, H. B. Yu, W. G. Yang, X. Liao, W. J. Tan, N. D. Jiao, Z. N. Wang and L. Q. Liu, *Biofabrication*, 2022, **14**, 025023.
100 C. Maggi, F. Saglimbeni, M. Dipalo, F. De Angelis and R. Di Leonardo, *Nat. Commun.*, 2015, **6**, 7855.
101 J. J. Abbott, Z. Nagy, F. Beyeler and B. J. Nelson, *IEEE Robot. Autom. Mag.*, 2007, **14**, 92–103.
102 K. B. Yesin, K. Vollmers and B. J. Nelson, *Int. J. Rob. Res.*, 2006, **25**, 527–536.
103 J. J. Abbott, K. E. Peyer, M. C. Lagomarsino, L. Zhang, L. Dong, I. K. Kaliakatsos and B. J. Nelson, *Int. J. Rob. Res.*, 2009, **28**, 1434–1447.
104 X. Yan, Q. Zhou, J. Yu, T. Xu, Y. Deng, T. Tang, Q. Feng, L. Bian, Y. Zhang, A. Ferreira and L. Zhang, *Adv. Funct. Mater.*, 2015, **25**, 5333–5342.

105 Z. Li, J. J. Abbott, L. Dong, B. E. Kratochvil, D. Bell and B. J. Nelson, *Appl. Phys. Lett.*, 2009, **94**, 064107.
106 T. Honda, K. I. Arai and K. Ishiyama, *IEEE Trans. Magn.*, 1996, **32**, 5085–5087.
107 X. Yang, W. F. Shang, H. J. Lu, Y. T. Liu, R. Tan, X. Y. Wu and Y. J. Shen, *Sci. Robot.*, 2020, **5**, eabc8191.
108 Y. Alapan, U. Bozuyuk, P. Erkoc, A. C. Karacakol and M. Sitti, *Sci. Robot.*, 2020, **5**, eaba5726.
109 K. W. Gyak, S. Jeon, L. Ha, S. Kim and D. Kim, *Adv. Healthcare Mater.*, 2019, **8**, 1900739.
110 S. Lee, S. Kim, S. Kim, J. Young, C. Moon, B. J. Nelson and H. Choi, *Adv. Healthcare Mater.*, 2018, **7**, 1700985.
111 J. Park, C. Jin, S. Lee, J. Y. Kim and H. Choi, *Adv. Healthcare Mater.*, 2019, **8**, 1900213.
112 H.-F. Xu, M. Medina-Sánchez, V. Magdanz, L. Schwarz, F. Hebenstreit and O.-G. Schmidt, *ACS Nano*, 2018, **12**, 327–337.
113 C. Peters, O. Ergeneman, P.-D. Wendel García, M. Müller, S. Pané, B. J. Nelson and C. Hierold, *Adv. Funct. Mater.*, 2014, **24**, 5269–5276.
114 S. Jeon, S. Kim, S. Ha, S. Lee, E. Kim, S. Y. Kim, S. H. Park, J. H. Jeon, S. W. Kim, C. Moon, B. J. Nelson, J. Y. Kim, S. W. Yu and H. Choi, *Sci. Robot.*, 2019, **4**, eaav4317.
115 D. Lin, N. Jiao, Z. Wang and L. Liu, *IEEE Robot. Autom. Lett.*, 2021, **6**, 2485–2492.
116 D. Lin, J. Wang, N. Jiao, Z. Wang and L. Liu, *Adv. Intell. Syst.*, 2021, **3**, 2000211.
117 X. Fan, X. Dong, A. C. Karacakol, H. Xie and M. Sitti, *Proc. Natl. Acad. Sci. U. S. A.*, 2020, **117**, 27916–27926.
118 C. A. Koepele, M. Guix, C.-H. Bi, G. Adam and D. J. Cappelleri, *Adv. Intell. Syst.*, 2020, **2**, 1900147.
119 T.-Y. Huang, F. Qiu, H.-W. Tung, K. E. Peyer, N. Shamsudhin, J. Pokki, L. Zhang, X.-B. Chen, B. J. Nelson and M. S. Sakar, *RSC Adv.*, 2014, **4**, 26771–26776.
120 T.-Y. Huang, M. S. Sakar, A. Mao, A. J. Petruska, F. Qiu, X.-B. Chen, S. Kennedy, D. Mooney and B. J. Nelson, *Adv. Mater.*, 2015, **27**, 6644–6650.
121 X. Dong and M. Sitti, *Int. J. Rob. Res.*, 2020, **39**, 617–638.
122 J. Yu, B. Wang, X. Du, Q. Wang and L. Zhang, *Nat. Commun.*, 2018, **9**, 3260.
123 B. Wang, K. F. Chan, J. Yu, Q. Wang, L. Yang, P. W. Y. Chiu and L. Zhang, *Adv. Funct. Mater.*, 2018, **28**, 1705701.
124 H. Xie, M.-M. Sun, X.-J. Fan, Z.-H. Lin, W.-N. Chen, L. Wang, L.-X. Dong and Q. He, *Sci. Robot.*, 2019, **4**, eaav8006.
125 T. Xu, G. Hwang, N. Andreff and S. Régnier, *IEEE Trans. Robot.*, 2015, **31**, 117–127.
126 T. Wei, J. Liu, D. Li, S. Chen, Y. Zhang, J. Li, L. Fan, Z. Guan, C. Lo, L. Wang, K. Man and D. Sun, *Small*, 2020, **16**, 1906908.
127 N. Ebrahimi, C. Bi, D. J. Cappelleri, G. Ciuti, A. T. Conn, D. Faivre, N. Habibi, A. Hoovsk, V. Iacovacci and I. Khalil, *Adv. Funct. Mater.*, 2020, **31**, 2005137.
128 H. J. Lu, M. Zhang, Y. Yang, Q. Huang, T. Fukuda, Z. Wang and Y. J. Shen, *Nat. Commun.*, 2018, **9**, 3944.
129 X. Wang, M. Luo, H. Wu, Z. Zhang, J. Liu, Z. Xu, W. Johnson and Y. Sun, *IEEE Trans. Robot.*, 2017, **34**, 240–247.
130 D. Li, F. Niu, J. Li, X. Li and D. Sun, *IEEE Trans. Ind. Electron.*, 2019, **67**, 4700–4710.
131 J.-Y. Li, X.-J. Li, T. Luo, R. Wang, C.-C. Liu, S.-X. Chen, D.-F. Li, J.-B. Yue, S.-H. Cheng and D. Sun, *Sci. Robot.*, 2018, **3**, eaat8829.
132 Y.-F. Si, J.-L. Hu and Z.-C. Dong, *Cell Rep. Phys. Sci.*, 2021, **2**, 100439.
133 J. S. Randhawa, T. G. Leong, N. Bassik, B. R. Benson, M. T. Jochmans and D. H. Gracias, *J. Am. Chem. Soc.*, 2008, **130**, 17238–17239.
134 Q. Jin, Y. Yang, J. A. Jackson, C. Yoon and D. H. Gracias, *Nano Lett.*, 2020, **20**, 5383–5390.
135 W. Wang, J. Giltinan, S. Zakharchenko and M. Sitti, *Sci. Adv.*, 2017, **3**, 1602522.
136 J. Yu, Q. Wang, M. Li, C. Liu, L. Wang, T. Xu and L. Zhang, *IEEE Robot. Autom. Lett.*, 2019, **4**, 2942–2949.
137 E. Diller and M. Sitti, *Adv. Funct. Mater.*, 2014, **24**, 4397–4404.
138 Z.-Q. Zheng, H.-P. Wang, L.-X. Dong, Q. Shi, J.-N. Li, T. Sun, Q. Huang and T. Fukuda, *Nat. Commun.*, 2021, **12**, 411–422.
139 Q. Wang, K. F. Chan, K. Schweizer, X. Du, D. Jin, S. C. H. Yu, B. J. Nelson and L. Zhang, *Sci. Adv.*, 2021, **7**, eabe5914.
140 E. M. Purcell, Life at low Reynolds number, *Am. J. Phys.*, 1977, **45**, 3–11.
141 N. Shamsudhin, V. I. Zverev, H. Keller, S. Pane, P. W. Egolf, B. J. Nelson and A. M. Tishin, *Med. Phys.*, 2017, **44**, e91–e111.
142 C. Heunis, J. Sikorski and S. Misra, *IEEE Robot. Autom. Mag.*, 2018, **25**, 71–82.
143 J. Hwang, J. Y. Kim and H. Choi, *Intell. Serv. Robot.*, 2020, **13**, 1–14.
144 X. Z. Chen, M. Hoop, F. Mushtaq, E. Siringil, C. Hu, B. J. Nelson and S. Pané, *Appl. Mater. Today*, 2017, **9**, 37–48.
145 T. Xu, Z. Hao, C. Huang, J. Yu, L. Zhang and X. Wu, *IEEE ASME Trans. Mechatron.*, 2022, DOI: **10.1109/TMECH.2022.3155806**.
146 G. Z. Lum, Z. Ye, X. Dong, H. Marvi, O. Erin, W. Hu and M. Sitti, *Proc. Natl. Acad. Sci. U. S. A.*, 2016, **113**, E6007–E6015.
147 X. Yang, R. Tan, H. Lu, T. Fukuda and Y. Shen, *Nat. Commun.*, 2022, **13**, 4156.
148 T. Xu, J. Zhang, M. Salehizadeh, O. Onaizah and E. Diller, *Sci. Robot.*, 2019, **4**, eaav4494.
149 S. Kim, S. Lee, J. Lee, B. J. Nelson, L. Zhang and H. Choi, *Sci. Rep.*, 2016, **6**, 30713.
150 T. Li, J. Li, H. Zhang, X. Chang, W. Song, Y. Hu, G. Shao, E. Sandraz, G. Zhang, L. Li and J. Wang, *Small*, 2016, **12**, 6098–6105.
151 L. Xing, P. Liao, H. Mo, D. Li and D. Sun, *IEEE Access*, 2021, **9**, 29279–29292.
152 Z.-Y. Ren, W.-Q. Hu, X.-G. Dong and M. Sitti, *Nat. Commun.*, 2019, **10**, 2703–2714.
153 J. Yu, L. Yang and L. Zhang, *Int. J. Rob. Res.*, 2018, **37**, 912–930.
154 T. Li, A. Zhang, G. Shao, M. Wei, B. Guo, G. Zhang, L. Li and W. Wang, *Adv. Funct. Mater.*, 2018, **28**, 1706066.
155 D. Ahmed, T. Baasch, N. Blondel, N. Laubli, J. Dual and B. J. Nelson, *Nat. Commun.*, 2017, **8**, 770.

156 F. Martinez-Pedrero and P. Tierno, *Phys. Rev. Appl.*, 2015, **3**, 051003.
157 H. Massana-Cid, F. Meng, D. Matsunaga, R. Golestanian and P. Tierno, *Nat. Commun.*, 2019, **10**, 2444.
158 D.-D. Jin, J.-F. Yu, Y. Ke and L. Zhang, *ACS Nano*, 2019, **13**, 5999–6007.
159 Z. Yang and L. Zhang, *Adv. Intell. Syst.*, 2020, **2**, 2000082.
160 M. P. Armacost, J. Adair, T. Munger, R. R. Viswanathan, F. M. Creighton, D. T. Curd and R. Sehra, *J. Cardiovasc. Electrophysiol.*, 2007, **18**, S26–S31.
161 D. Folio and A. Ferreira, *IEEE Trans. Robot.*, 2017, **33**, 583–593.
162 B. L. Nguyen, J. L. Merino and E. S. Gang, *Eur. Cardiol.*, 2010, **6**, 50–56.
163 J. Li, B. E. F. de Ávila, J. Li, W. Gao, L. Zhang and J. Wang, *Sci. Robot.*, 2017, **2**, eaam6431.
164 J. Vialetto, M. Hayakawa, N. Kavokine, M. Takinoue, S. N. Varanakkottu, S. Rudiuk, M. Anyfantakis, M. Morel and D. Baigl, *Angew. Chem., Int. Ed.*, 2017, **56**, 16565–16570.
165 W. Amokrane, K. Belharet, M. Souissi, G. A. Bozorg and A. Ferreira, *Rob. Auton. Syst.*, 2018, **107**, 10–19.
166 L. Yang, L. Gen, H. J. Lu, Y. Y. Yang, Z. Y. Liu, W. F. Shang and Y. J. Shen, *ACS Appl. Mater. Interfaces*, 2019, **11**(29), 25664–25673.
167 T. Xu, Y. Guan, J. Liu and X. Wu, *IEEE Trans. Autom. Sci. Eng.*, 2020, **17**, 325–333.
168 S. Xu, J. Liu, C. Yang, X. Wu and T. Xu, *IEEE Trans. Cybern.*, 2022, **52**, 13727–13737.
169 M. P. Kummer, J. J. Abbott, B. E. Kratochvil, R. Borer, A. Sengul and B. J. Nelson, *IEEE Trans. Robot.*, 2010, **26**, 1006–1017.
170 E. Diller, J. Giltinan, G. Z. Lum, Z. Ye and M. Sitti, *Int. J. Robot. Res.*, 2016, **35**, 114–128.
171 D. Liu, X. Liu, Z. Chen, Z. Zuo, X. Tang, Q. Huang and T. Arai, *Cyborg Bionic Syst.*, 2022, **2022**, 9850832.
172 F. Liu, X. Liu, Q. Huang and T. Arai, *Cyborg Bionic Syst.*, 2022, **2022**, 9758460.
173 Z. Ye and M. Sitti, *Lab Chip*, 2014, **14**, 2177–2182.
174 D. Zhong, W. Li, Y. Qi, J. He and M. Zhou, *Adv. Funct. Mater.*, 2020, **30**, 1910395.
175 K. Villa, J. Vyskocil, Y. Ying, J. Zelenka and M. Pumera, *Chem. – Eur. J.*, 2020, **26**, 3039–3043.
176 J. Xing, T. Yin, S. Li, T. Xu, A. Ma, Z. Chen, Y. Luo, Z. Lai, Y. Lv, H. Pan, R. Liang, X. Wu, M. Zheng and L. Cai, *Adv. Funct. Mater.*, 2021, **31**, 2008262.
177 A. G. Guex, N. Di Marzio, D. Eglin, M. Alini and T. Serra, *Mater. Today Bio*, 2021, **10**, 100110.
178 X. Wang, J. Cai, L. Sun and D. Zhang, *ACS Appl. Mater. Interfaces*, 2019, **11**, 4745–4756.
179 B. Han, Y. Gao, Y. L. Zhang and H. B. Sun, *Nano Energy*, 2020, **71**, 104578.
180 D. Zhong, W. Li, Y. Qi and M. Zhou, *Adv. Funct. Mater.*, 2020, **30**, 1910395.
181 M. Pilz Da Cunha, Y. Foelen, R. J. H. van Raak and A. P. H. J. Schenning, *Adv. Opt. Mater.*, 2019, **7**, 1801643.
182 H. Zhou, G. Dong, G. Gao, R. Du, X. Tang, Y. Ma and J. Li, *Cyborg Bionic Syst.*, 2022, **2022**, 9852853.
183 J. Li, L. Dekanovsky, B. Khezri, B. Wu, H. Zhou and Z. Sofer, *Cyborg Bionic Syst.*, 2022, **2022**, 9824057.

